# Integrated Inductors with Micro-Patterned Magnetic Thin Films for RF and Power Applications

by

Hao Wu

A Dissertation Presented in Partial Fulfillment
of the Requirements for the Degree
Doctor of Philosophy

Approved November 2013 by the
Graduate Supervisory Committee:

Hongbin Yu, Chair
Bertan Bakkaloglu
Yu Cao
Shamala Chickamenahalli

ARIZONA STATE UNIVERSITY

December 2013

ABSTRACT

With increasing demand for System on Chip (SoC) and System in Package (SiP) design in computer and communication technologies, integrated inductor which is an essential passive component has been widely used in numerous integrated circuits (ICs) such as in voltage regulators and RF circuits. In this work, soft ferromagnetic core material, amorphous Co-Zr-Ta-B, was incorporated into on-chip and in-package inductors in order to scale down inductors and improve inductors performance in both inductance density and quality factor.

With two layers of 500 nm Co-Zr-Ta-B films a 3.5X increase in inductance and a 3.9X increase in quality factor over inductors without magnetic films were measured at frequencies as high as 1 GHz. By laminating technology, up to 9.1X increase in inductance and more than 5X increase in quality factor (Q) were obtained from stripline inductors incorporated with 50 nm by 10 laminated films with a peak Q at 300 MHz. It was also demonstrated that this peak Q can be pushed towards high frequency as far as 1GHz by a combination of patterning magnetic films into fine bars and laminations. The role of magnetic vias in magnetic flux and eddy current control was investigated by both simulation and experiment using different patterning techniques and by altering the magnetic via width. Finger-shaped magnetic vias were designed and integrated into on-chip RF inductors improving the frequency of peak quality factor from 400 MHz to 800 MHz without sacrificing inductance enhancement. Eddy current and magnetic flux density in different areas of magnetic vias were analyzed by HFSS 3D EM simulation. With optimized magnetic vias, high frequency response of up to 2 GHz was achieved.

Furthermore, the effect of applied magnetic field on on-chip inductors was investigated for high power applications. It was observed that as applied magnetic field along the hard axis (HA) increases, inductance maintains similar value initially at low fields, but decreases at larger fields until the magnetic films become saturated. The high frequency quality factor showed an opposite trend which is correlated to the reduction of ferromagnetic resonant absorption in the magnetic film. In addition, experiments showed that this field-dependent inductance change varied with different patterned magnetic film structures, including bars/slots and fingers structures.

Magnetic properties of Co-Zr-Ta-B films on standard organic package substrates including ABF and polyimide were also characterized. Effects of substrate roughness and stress were analyzed and simulated which provide strategies for integrating Co-Zr-Ta-B into package inductors and improving inductors performance. Stripline and spiral inductors with Co-Zr-Ta-B films were fabricated on both ABF and polyimide substrates. Maximum 90% inductance increase in hundreds MHz frequency range were achieved in stripline inductors which are suitable for power delivery applications. Spiral inductors with Co-Zr-Ta-B films showed 18% inductance increase with quality factor of 4 at frequency up to 3 GHz.

## DEDICATION

This dissertation is dedicated to my loving parents, Mr. Kailiang Wu (吴开亮) and Mrs. Shaocui Zhang (张绍翠), who have given me the opportunity of an education from the best institutions and support throughout my life.

ACKNOWLEDGMENTS

I would like to express the deepest appreciation to my committee chair, Professor Hongbin Yu, who continually and convincingly convey a spirit of adventure in regard to research and scholarship, and an excitement in regard to teaching. Without his guidance and persistent help this dissertation would not have been possible.

I would like to thank my committee members, Professor Bertan Bakkaloglu, Professor Yu Cao, Professor Shimeng Yu and Dr. Shamala Chickamenahalli for providing guidance and helpful discussions. I also thank Dr. Donald Gardner from Intel, who not only helps deposit the magnetic materials but also shares his expertise on integrated magnetic thin film inductors.

I would like to thank members past and present of Dr. Hongbin Yu's research group for their help and support, especially Dr. Wei Xu, from whom I learned lots of semiconductor fabrication techniques. Thanks also go out to Dr. Nicholas Rizzo and his group members in Everspin for providing measurement facilities and valuable suggestions. I would also like to take this opportunity to thank all the staff of ASU NanoFab for their support.

Finally, but most importantly, I would like to thank my parents and Yiran Li for their love, encouragement, patience, understanding and support throughout the entire doctorate program. They have been my cheerleaders so that I could overcome the difficulties during these years.

TABLE OF CONTENTS

Page

CHAPTER Page

CHAPTER Page

LIST OF TABLES

Table Page

LIST OF FIGURES

Figure Page

Figure Page

Figure Page

Figure Page

Figure Page

LIST OF SYMBOLS

Symbol Page

# Chapter 1

# INTRODUCTION

## 1.1 Background and Motivation

Inductors are essential passive components widely-used in numerous electronic circuits such as in radio-frequency (RF), microwave, voltage regulators and power delivery circuits. With the ongoing drive toward miniaturization of electronic products, with ever-increasing functionality and performance, from portable electronics to high-end computing, inductors has constantly evolved from early discrete components on printed circuit boards (PCBs) to integrated ones in package or on Si chip. [1-5] Such integration of inductors is the prerequisite to the implementation of System in Package (SiP), System on Chip (SoC), Power Supply in Package (PwrSiP) and Power Supply on Chip (PwrSoC) design in computer and communication technologies, such as multi-core processor and portable and low-power consumption wireless devices. [6-9]

However, among all the fundamental components inductors are least compatible with silicon integration with some substantial disadvantages, e.g. large silicon area consumption, high substrate loss, high DC resistance and high cost. Large size integrated air-core planar spiral inductors used today usually occupy precious chip area which does not scale efficiently with the number of turns. Besides, due to a electric-magnetic coupling with the conductive silicon substrate integrated inductors perform poorly, with quality factors Q of 3 being usual. High quality factor is required since it directly impacts the phase noise of the frequency synthesizer and directly affects the wireless channels spacing and frequency planning. To simultaneously achieve high inductance density and quality factor, ferromagnetic core material have been incorporated into on-chip inductors

which has become increasingly attractive particularly in RF/microwave integrated circuits and power electronics applications. Furthermore, with ferromagnetic materials, on-chip inductors tend to cause less electromagnetic interference (EMI) to the other analogue/digital circuit blocks within close proximity.

Besides the on-chip inductors, in-package or on-package inductors have also attracted many research interests since moving the inductors from the die to the package substrate would reduce the die size and cost. Thanks to the advanced packaging technologies, in-package inductors using multi-levels of metals are feasible and superior in quality factor compared to on-chip inductors.

**1.2 Review of Previous Work**

Much research has been carried out to fabricate and integrate high inductance density and high quality factor inductors on silicon. For a magnetically enhanced on-chip inductor, a number of coil and winding geometries have been investigated including spiral, strip, toroidal, solenoid and meander structures. Among all these structures, spiral inductors are commonly used in COMS technology due to their low profile and well-developed integrated fabrication process. Monolithic on-chip air-core inductors in current CMOS RF circuits consisting of a spiral geometry are fabricated using high levels of metals without magnetic materials and exhibit inductances ranging from 1-10 nH. They occupy a large substrate area with inductance densities lower than 100 $nH/mm^2$.[8] Stacked or 3D structures are proposed to reduce the area of on-chip spiral inductors in which spiral inductors in different metal layers are series-connected. Though the inductance is enhanced, the quality factor and the resonant frequency sacrifice due to higher series resistance and larger parasitic capacitance.[10-13] A more effective way to

increase inductance and quality factor along with reducing capacitance, resistance, and size can be achieved by adopting magnetic materials in integrated inductors which greatly benefit integrated circuits design. [14, 15]

Considering the large chip area occupied by on-chip inductor with air core, use of magnetic films as flux-amplifying components yields smaller inductors. A lot of designs have been researched with most of the flux contained within the magnetic films, which also reduces unwanted losses in the silicon substrate. Over the last 20-30 years enormous efforts have been made to fabricate an efficient CMOS-compatible magnetic inductor and extend its operating frequency range from 1-10 MHz to 100-1000 MHz. A few representative works are briefly reviewed here with a focus on on-chip spiral inductors. Limited increases in inductance (30-60%) have been demonstrated by depositing a single layer of magnetic material over spiral inductors.[16-18] The theoretical limit for a single level of magnetic material deposited over spiral or stripe inductors is only a 2X (or 100%) increase. Although simulations of inductors using two layers of magnetic material have suggested that large increases (7-fold) in inductance are possible, it has proven difficult to achieve. Shirae and coworkers have implemented a number of structures with planar coils embedded in $SiO_2$ and sandwiched between two Ni-Fe films.[19] However, this design yielded a low efficiency (Q=1) and the resonances are only at a few tens of MHz which were attributed to the distributed coil/SiO2/film capacitance in the structure. Furthermore, by changing the magnetically sandwiched spiral inductor structure into stripeline, the high frequency response of the magnetic inductor can be improved with $Q > 3$ at 100 MHz. However, the enhancement of the inductance is very small.[20] Regarding this problem, the importance of flux closures at the edges of the conductor was pointed out

first by Oshiro.[21] Yamaguchi et al.[22] have demonstrated a gain in inductance up to a factor of 4 with Q~2-3 at 100 MHz by using Ni-Fe-coated conductor strips, with and without magnetic closures at the edges. Additionally, Cu strips sandwiched with Ni-Fe and Co-Nb-Zr, with and without flanges at the edges, have been carefully studied by Korenivski and Van Dover.[23] By varying the width of the stripeline from 10-50 μm, the results showed up to 7X enhancements of inductance over the air-core value (100 nH/cm linear inductance density) with Q < 2 at frequencies up to 250 MHz. Some studies have focused on obtaining high peak Q-factors based on structures chosen already with higher peak Q-factors prior to adding magnetic material thanks to the high frequency they were designed for, but the gains in inductance were only 8% - 30%.[18, 24, 25] Recently, Gardner and co-workers have demonstrated ~31X increase of inductance by using flux-closed double-layer Co-Zr-Ta magnetic material integrated spiral inductors.[26] Inductance densities of up to 1700 $nH/mm^2$ and quality factors of up to 8 were obtained. However, the working frequency was limited up to 40 MHz, which prevents its usage in RFIC. Soft ferrites are another alternatives which are attractive for their high resistivity. Compared with magnetic alloys, low saturation magnetization and high process temperature are the main disadvantages of ferrites. Typical permeability of ferrites obtained by sol-gel spin-coating is around 10-30.[27] Therefore, inductance increase is not so significant that the added cost of using magnetic material seems not worthwhile. Besides the materials mentioned above, other ferromagnetic materials, such as Co-Nb-Zr [28], Fe-Hf-N [29], Fe-Co-$SiO_2$ [30], Fe-Co-Ta-N [31] and Fe-Ta-N [32, 33], have also been implemented into on-chip inductors aiming for different applications.

Other than planar spiral structures, a solenoid inductor with laminated amorphous magnetic cores (Co-Fe-Si-B) was studied by Shirakawa [34, 35], which demonstrated up to 10-fold enhancement of inductance with Q = 2 at frequency of 10-100 MHz. The solenoid structure has its advantages in fully utilizing the hard axis of the magnetic core since the induced magnetic field is always along its axial direction. Zhuang [36] fabricated solenoid inductors with Ni-Fe magnetic core achieving more than 20-fold enhancement of inductance. Solenoid inductors fabricated on PCB with CoFeHfO magnetic cores were reported by Shan Wang's group [37] from Stanford University and the similar structure was also used for integrated transformers in their recent published paper. [38] Another type of inductors attracting research interest is toroidal inductor. [13] But the need of control magnetic anisotropy in magnetic core's radial direction jeopardizes the implementation of magnetic materials and the relatively complicated process makes toroidal inductor not suitable for on-chip applications. [39]

### 1.3 Organization

Following this chapter, chapter 2 includes the preparation and characterization of amorphous Co-Zr-Ta-B as well as 80%Ni-20%Fe which is one of common used soft ferromagnetic materials known as Permalloy. Patterning effects in magnetic films are also investigated in this chapter. By calculating the demagnetizing factor, aspect ratio dependence of saturation field in micro-patterned magnetic bars is analyzed.

Chapter 3 presents simulation results from 3D electromagnetic simulator ANSYS HFSS. Based on simulations, optimizations of on-chip inductor design have been applied for achieving higher inductance and higher quality factor. Optimized parameters include

copper thickness, magnetic thin film thickness, space between copper and magnetic materials, etc.

Chapter 4 demonstrates the experimental work on on-chip magnetic thin film inductors with amorphous Co-Zr-Ta-B. Stripline and spiral inductors were designed and fabricated with different combinations of laminated Co-Zr-Ta-B films. Measurement results show superior frequency performance of inductors with laminated patterned films.

In Chapter 5 the role of magnetic vias in magnetic flux and eddy current control was investigated by both simulation and experiment. Different patterning techniques and varied via width were utilized to improve the inductor RF performance. The magnetic flux path in magnetic films was examined by 3D EM simulation based on which finger-shaped magnetic vias were improved by elaborately keeping the magnetic flux path continuous around the copper coils.

Chapter 6 investigated the effect of applied field on on-chip inductors which is one of concerns in high power density applications. An efficient way to accurately evaluate magnetic thin film is tested and verified. The saturation field of inductors is effectively tuned by different patterning of magnetic films.

Chapter 7 characterized the magnetic properties of magnetic films on organic packaging substrates including ABF and polyimide substrates. Experiments on in-package inductors with integrated magnetic materials show promising applications in Power Supply in Package design.

Chapter 8 summarizes the major contributions of this dissertation and suggests areas that merit future work.

# Chapter 2

# MAGNETIC THIN FILM CHARACTERIZATIONS AND PATTERNING EFFECTS IN MICRO-PATTERNED FILMS

## 2.1 Magnetic Material Requirements for Inductor Applications

Ideal ferromagnetic materials which can be integrated into on-chip inductors should have large permeability, low magnetic loss in the operating frequency range, and CMOS process compatibility. These three criteria assure that such ferromagnetic materials are helpful for large inductance increase, large quality factor and process feasibility. From the engineer point of view, each requirement can be further subdivided into the following items.

(1) High saturation magnetization, $M_s$. This requirement is obvious. Since the magnetic film is used as flux amplifier, the higher the permeability, the larger increase in inductance. Considering that the easy axis of magnetic material is saturated at relatively small external magnetic field, most of the designs are expected to employ the transverse (hard axis) permeability in films of uniaxial anisotropy, which is directly proportional to $M_s$: $\mu \cong 4\pi M_s/H_k$, where $H_k$ is the anisotropy field.

(2) High ferromagnetic resonant frequency (FMR). At FMR the magnetic moments in ferromagnetic films process at the resonant frequency resulting in dramatically absorption of RF energy. The permeability turns out mostly imaginary, which would make an inductor into a resistor. FMR is determined by the Kittel equation[40] as

$$f_r = \frac{\gamma}{2\pi}\sqrt{\frac{M_s H_k}{\mu_0}} \quad (1)$$

Increasing anisotropy field $H_k$ can achieve higher FMR with the drawback of lower permeability.

(3) High resistivity, ρ. Eddy currents are one of the most important energy loss mechanisms especially at high frequency end. Ferromagnetic materials which are usually metal alloys are good conductors for eddy currents. High resistivity can help reduce the eddy current loss leading to a high quality factor.

(4) Single domain state, for low magnetic loss as well as for reproducibility. Variations in inductance caused by changes in the domain pattern of the magnetic films is usually unacceptable in a commercial product;

(5) Low magnetostriction. Since the fabrication process may result in stress in the films leading to stress-induced anisotropy, therefore limiting the permeability, it is preferred that the magnetic material has as small magnetostriction as possible.

(6) Low preparation temperature. CMOS compatibility of magnetic materials and their incorporation process is also critical for the application of the magnetic inductors. A restricted process temperature required for other on-chip components, preferably less than 200 $^{o}$C.

**2.2 Characterizations of laminated Ni-Fe thin films**

Ni-Fe is one of the most common used soft magnetic alloys which can be found in many electrical equipments as magnetic cores. Although electroplating is a more economic way to deposit Ni-Fe, insulation layers cannot be deposited by electroplating to form laminated films. *Wei et al.*[41, 42] sputtered laminated Ni-Fe films with thin chromium layers as insulation layers and observed tuned permeability through changing the laminated layer thickness. To further improve film resistivity, $SiO_2$ was used to

replace the chromium layers. Laminated Ni-Fe films of 20 nm by 5 layers with 5 nm thick $SiO_2$ insulations in between were deposited by Lesker sputtering system. The base pressure was 1 x $10^{-6}$ torr and sputter pressure was maintained at 4 mtorr using Ar at 200 W of DC power for Ni-Fe. The power was kept constant to maintain a constant deposition rate of 1.5 Å/s. The substrate was rotated at a constant rate of 30 rpm to ensure the uniformity of the deposited film. An external DC magnetic field of 400 Oe was applied during the sputtering to render unaxial anisotropy. Fig. 1 shows the measured hysteresis loops from Ni-Fe films on quartz, ABF and polyimide substrates. Magnetic properties such as coercivity $H_c$ and anisotropy field $H_k$ were extracted and listed in Table I.

Table I Material Properties of laminated Ni-Fe films

| | Quartz | ABF | Polyimide |
|---|---|---|---|
| $H_c$ (Oe) | 0.8 | 4.3 | 2 |
| $H_k$ (Oe) | 10 | 27 | 18 |

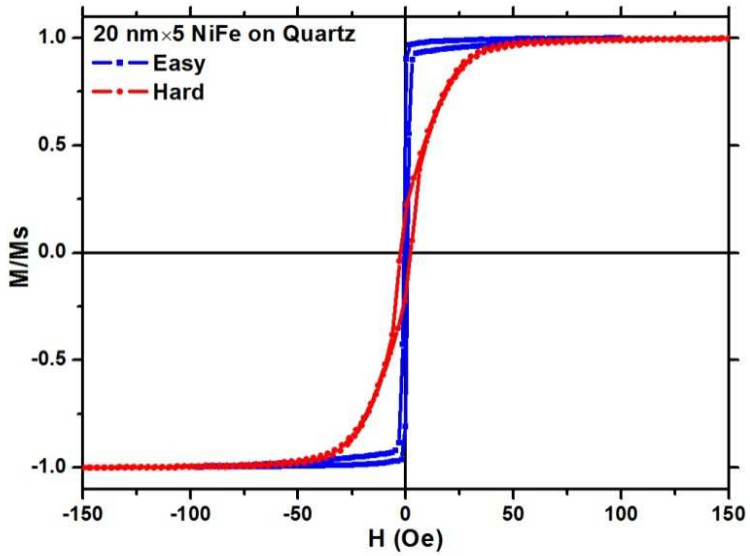


(a)

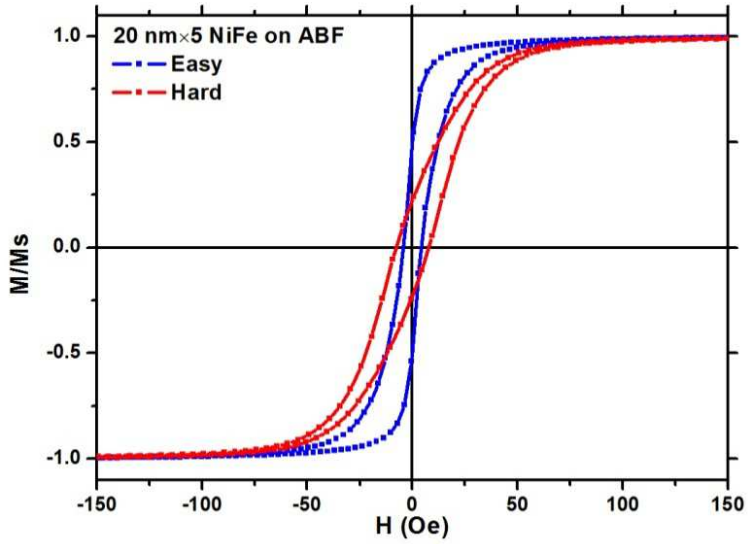


(b)

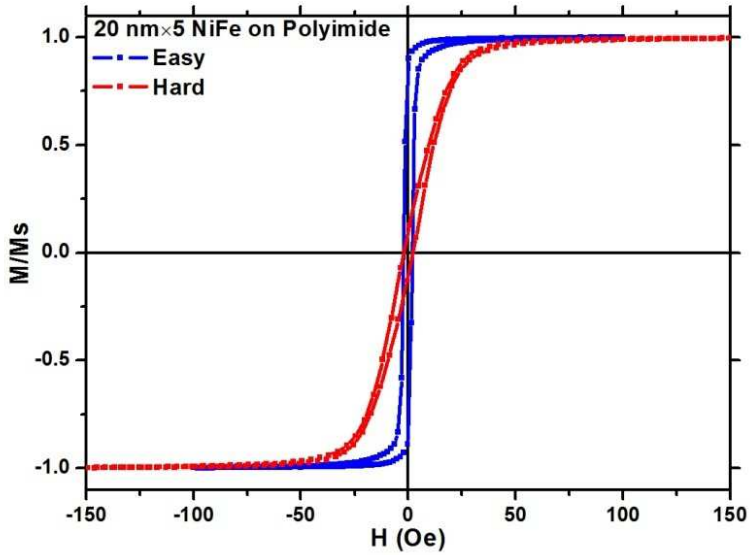


(c)

Fig. 1 Measured M-H hysteresis loops of laminated Ni-Fe films on (a) quartz (b) ABF (c) polyimide substrates.

### 2.3 Characterizations of laminated and non-laminated Co-Zr-Ta-B thin films

The amorphous Co-4%Zr-4%Ta-8%B (at. %) alloy was prepared by DC magnetron sputtering. Boron in Co-Zr-Ta-B is used to increase the resistivity of the material leading to lower induced eddy current. The resistivity of Co-Zr-Ta-B films was measured as 115

μΩ·cm, which is higher than Co-Zr-Ta's resistivity of 98 μΩ·cm. An external DC magnetic field was applied during the deposition to render the Co-Zr-Ta-B film magnetically anisotropic. A low-frequency permeability of 1070 Gauss/Oe along the hard axis was extracted from vibrating sample magnetometer (VSM) measured M-H hysteresis loop (Fig. 2) and the coercivity was less than 0.1 Oe resulting in low hysteretic losses. Using pulsed inductive microwave magnetometry (PIMM), the ferromagnetic resonant frequency (FMR) for a 500 nm thick Co-Zr-Ta-B film was found to be 1.6GHz at zero bias field and can be further increased by laminating or patterning the magnetic film. Main magnetic properties of Ni-Fe, Co-Zr-Ta and Co-Zr-Ta-B are listed in Table II for comparison.

Table II Comparison of Ni-Fe, Co-Zr-Ta and Co-Zr-Ta-B sputtered films

| | Ni-Fe [42] | Co-Zr-Ta [43] | Co-Zr-Ta-B |
|---|---|---|---|
| permeability, μ | 650 | 1000 | 2 |
| resistivity, ρ (μΩ·cm) | 20 | 100 | 115 |
| FMR (GHz) | 0.64 | 1.4 | 1.6 |

Cobalt oxide formed by introducing oxygen into sputtering system was used to laminate Co-Zr-Ta-B film. Two different laminated films, 100 nm by 5 and 50 nm by 10, were deposited onto spiral on-chip inductors as well as 500 nm thick non-laminated film.

M-H hysteresis loops of as-deposited Co-Zr-Ta-B films were measured by vibrating sample magnetometer (VSM) as seen in Fig. 2. Both the easy axis and hard axis coercivity values for laminated films are higher than that for a single layer film (see Fig. 2. insets). This is due to the interactions between each laminated layer where the magnetization of each layer is antiparallel aligned for minimum energy. For the same

reason, the anisotropy field $H_K$ increases with increasing number of lamination layers and decreasing laminations thickness, whereas from hard-axis M-H loop an $H_K$ near 25 Oe was deduced for 500 nm thick Co-Zr-Ta-B film and the 10 layers of 50 nm laminated film has the largest $H_K$ of 60 Oe. Though the low-frequency permeability ( $4\pi M_S / H_K$ ) of laminated films becomes lower due to the higher $H_K$, the laminated films are more suitable for high frequency applications as the ferromagnetic resonant frequency (FMR) which is proportional to $\sqrt{M_S H_K}$ increases.

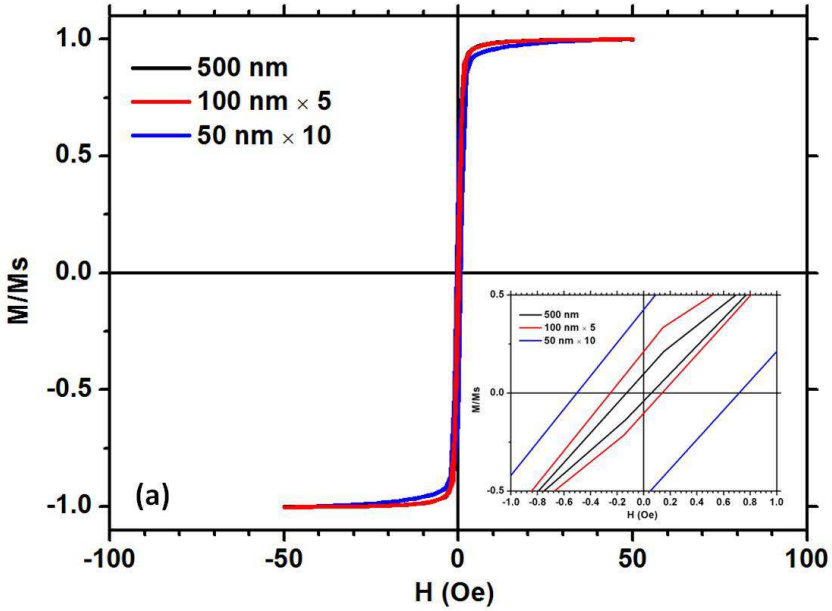


(a)

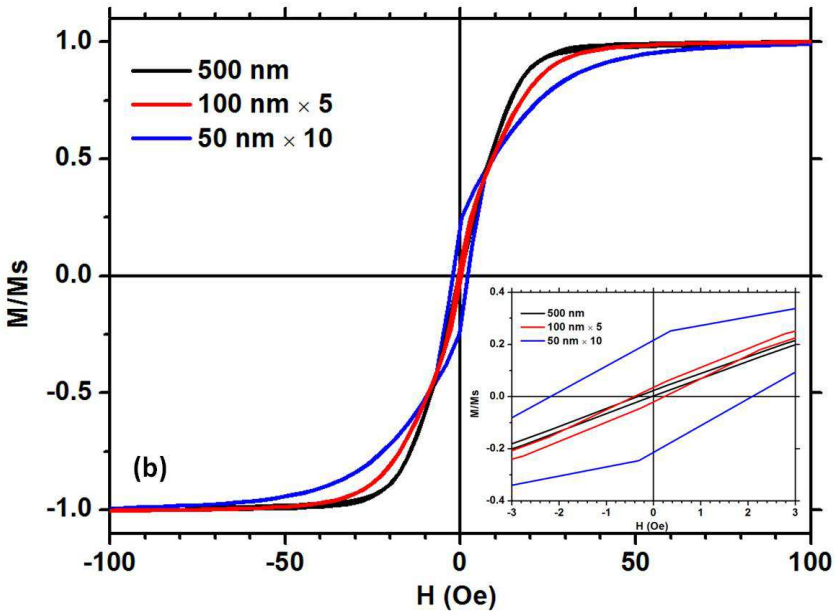


(b)

Fig. 2. M-H magnetic hysteresis loops of as-deposited Co-Zr-Ta-B films, (a) easy axis and (b) hard axis. Insets show the coercivity of each film.

### 2.4 Patterning Effects in Micro-patterned Co-Zr-Ta-B thin films

In on-chip inductor applications, magnetic films are usually patterned into arbitrary shapes for better inductor performance, i.e. large quality factor (Q) and high operating frequency. Experimental measurements, however, have shown that the magnetic film properties, such as coercivity ($H_c$) and permeability (μ), of those patterned magnetic films can differ from their intrinsic properties. The difference arises from changes of demagnetizing field, shape anisotropy energy, domain structure, etc. In patterned magnetic thin film with in-plane uniaxial anisotropy and single domain state, the most significant factor is the demagnetizing field. By adjusting the aspect ratio of width to length, inside demagnetizing field can be tuned leading to a tunable anisotropy field and saturation field. The saturation field ($H_{sat}$) is one of the most important

properties of patterned magnetic films for inductor applications, because it not only affect the effective permeability of patterned films but also determines the maximum current that inductors can undertake (large current will saturate the magnetic films leading to decreased inductance). In particular, in inductors with magnetic materials in voltage regulator application, large saturation field directly will lead to the large saturation current.[44, 45] Previous research on patterned magnetic films focus on theoretical analysis and experimental characterization without relating this adjustable saturation field to magnetic thin film inductor applications.

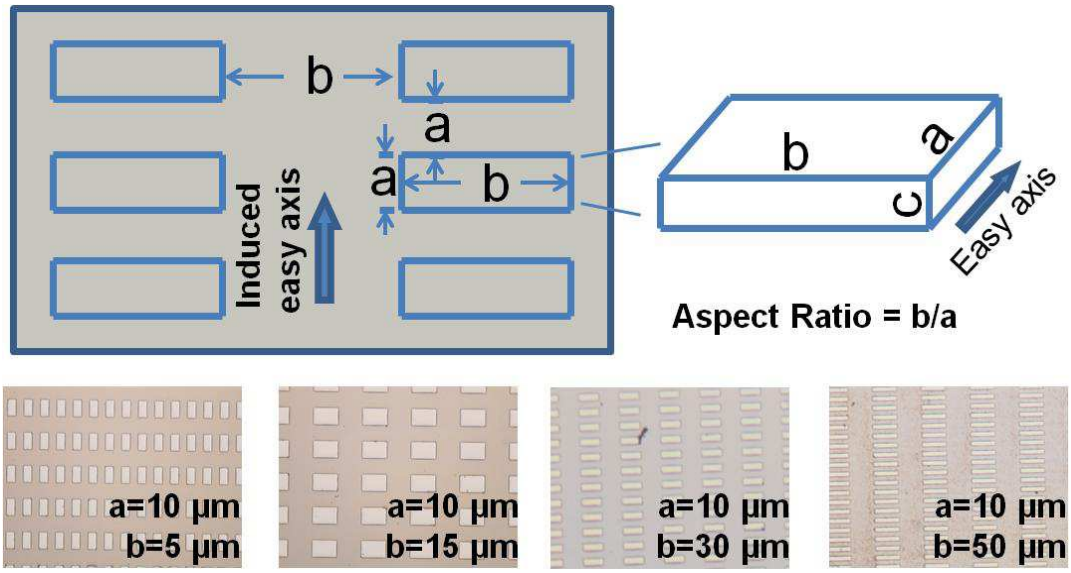


Fig. 3 Patterned Co-Zr-Ta-B films with different aspect ratio which is defined as the length in hard axis to the length in easy axis, i.e. b/a. Easy axis was induced by applied magnetic field during sputtering. Top: Schematic of the pattern. Bottom: optical images of patterned arrays with different aspect ratios of, from left to right, 1:2, 1.5:1, 3:1, and 5:1.

Electron beam lithography (EBL) was used for patterning. Fig. 3 shows the schematic and fabricated patterned Co-Zr-Ta-B magnetic bars array with different aspect

ratios. Every patterned array has 50/50 areal coverage ratio, i.e. the space is the same as the dimension of the magnetic bars in each direction.

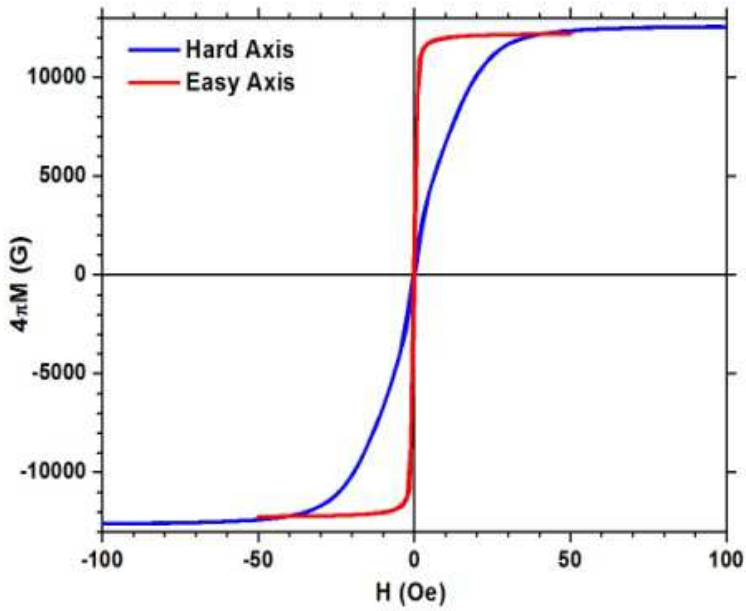


**(a)**

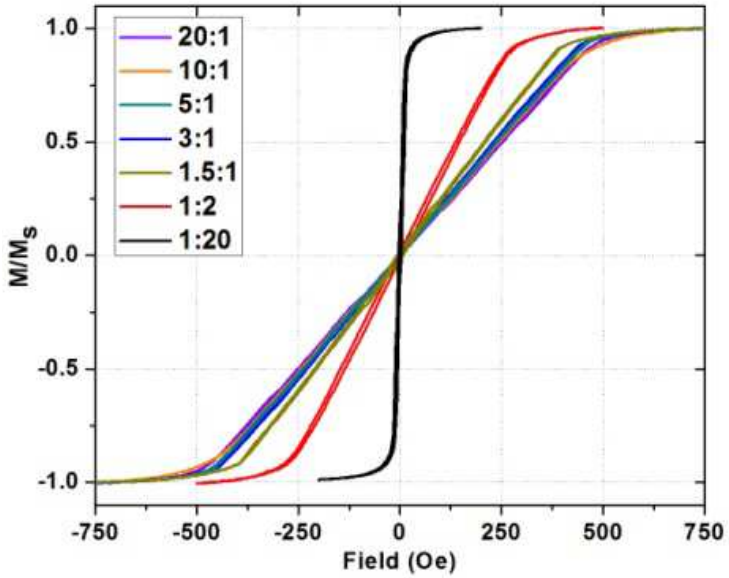


**(b)**

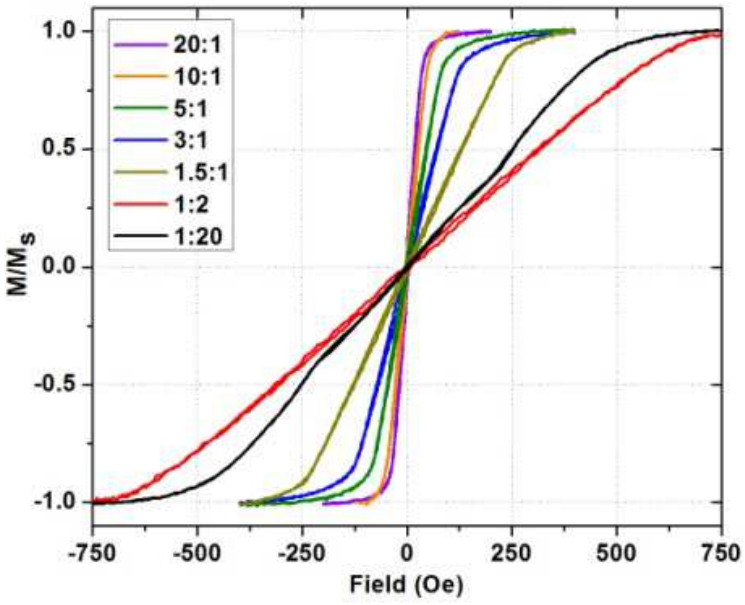


**(c)**

Fig. 4 Measured M-H hysteresis loop from 100 nm×5 laminated Co-Zr-Ta-B film. (a) 0.7 mm×0.7 mm un-patterned film. The saturation fields along easy and hard axis are 5 Oe and 35 Oe, respectively. (b) Easy Axis and (c) Hard Axis of patterned films with different aspect ratio. Aspect ratio is defined as the b/a, see Fig. 3.

The saturation field of un-patterned and patterned Co-Zr-Ta-B films were extracted from the M-H hysteresis loops shown in Fig. 4. The un-patterned film has a dimension of 0.7 mm by 0.7 mm showing an easy axis saturation field ($H_{sat\_E}$) of 5 Oe and a hard axis saturation field ($H_{sat\_H}$) of 35 Oe. As Co-Zr-Ta-B films were patterned into array of rectangular bars, both $H_{sat\_E}$, from 15 Oe to 500 Oe, and $H_{sat\_H}$, from 40 Oe to 655 Oe, increase significantly compared to un-patterned films due to increasing shape anisotropy energy, as listed in Table III. In addition, the saturation field shows clearly a dependency on the aspect ratio of the patterned magnetic bars. For the bars with large aspect ratio, the shape anisotropy energy overcomes the induced anisotropy from the applied field during deposition so that the intended easy axis direction has larger saturation field compared to that in the intended hard axis. In this sense, the easy axis and

hard axis have switched, which can be seen much clearly in the plot of saturation fields in both directions versus aspect ratio (Fig. 5). The switching of easy and hard axis occurs at around aspect ratio of 1, in the range and steps of aspect ratio change investigated in this work.

Table III. Saturation field, demagnetizing factors, $N_d$ and stray field factors, $N_s$

| Aspect ratio | $H_{sat\_E}$ (Oe)[a] | $H_{sat\_H}$ (Oe)[b] | $N_{d\_E}$ | $N_{d\_H}$ | $N_{s\_E}$ | $N_{s\_H}$ |
|---|---|---|---|---|---|---|
| 20:1 | 500 (338) | 40 (38) | 0.03093 | 0.00008 | 0.00432 | -0.00015 |
| 10:1 | 485 (327) | 55 (45) | 0.03023 | 0.00032 | 0.00447 | -0.00051 |
| 5:1 | 475 (307) | 85 (66) | 0.02876 | 0.00123 | 0.00460 | -0.00123 |
| 3:1 | 457 (289) | 142 (95) | 0.02692 | 0.00321 | 0.00423 | -0.00160 |
| 1.5:1 | 426 (255) | 265 (184) | 0.02290 | 0.01060 | 0.00292 | -0.00135 |
| 1:2 | 278 (207) | 655 (564) | 0.01316 | 0.04934 | -0.00307 | 0.00704 |
| 1:20 | 15 (8) | 500 (368) | 0.00008 | 0.03093 | -0.00015 | 0.00432 |

[a,b]Measured values (calculated values)

This aspect ratio dependence of saturation field arises from the shape dependence of demagnetizing field ($H_d$) in the patterned films which is calculated by $H_d = -MN_d$. $N_d$ is demagnetizing factor. There are two types of demagnetizing factors, i.e. the magnetometric demagnetizing factor [46] and the ballistic (fluxmetric) demagnetizing factor [47]. *Li et al.* [48] demonstrated that the latter is more suitable for soft magnetic thin films. As the interaction between adjacent magnetic bars in an array also contributes to the field distribution, the stray field of magnetic bars was calculated by a numerical

method [49]. Considering stray fields only from neighbor magnetic bars, the effective saturation field is given by $H_{sat\_eff} = H_{sat} + (N_d + N_s) \times M_s$. $N_s$ is the stray field factor. The calculated saturation field listed in Table III, shows better agreements with measured results, extracted from hysteresis loops in Fig. 4, in hard axis, and 60% to 70% accuracy in easy axis.

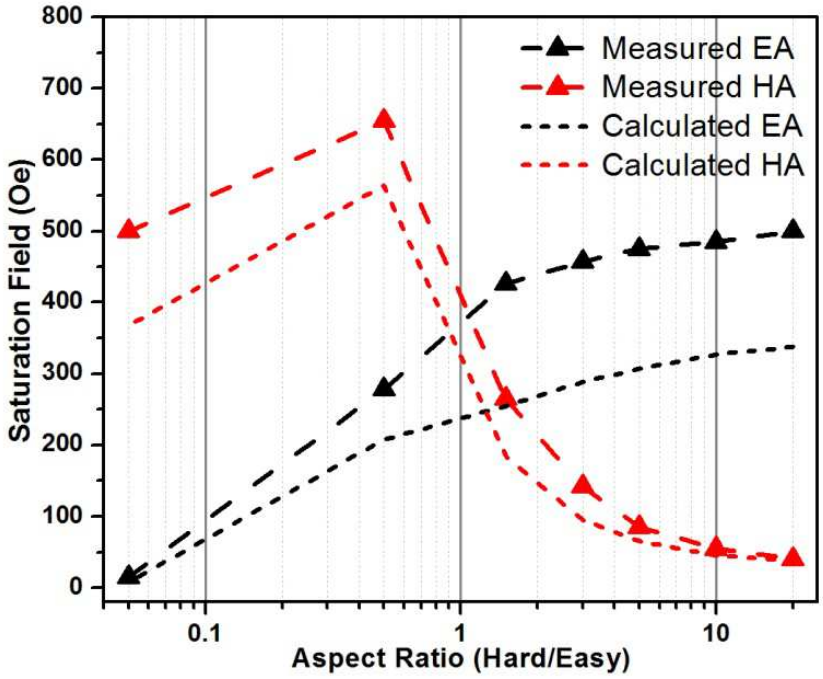


Fig. 5 Measured and calculated saturation filed of patterned magnetic bars array in easy axis (EA) and hard axis (HA).

## Chapter 3

## OPTIMIZATION OF INDUCTORS WITH MAGNETIC MATERIALS USING 3D ELECTROMAGNETIC SIMULATIONS

Electromagnetic simulation of magnetic inductor performance, including inductance, quality factor, and frequency response, with varying structural parameters is important for obtaining optimal design before experimental implementations. ANSYS HFSS which is a 3-D fullwave electromagnetic-field simulator has been used in radio frequency on-chip magnetic thin film inductors design to optimize both inductance and quality factor. Simulated and optimized parameters include copper thickness, magnetic film thickness, the space between copper coils and magnetic films, patterned shapes of magnetic vias and films. It is demonstrated in simulations that the quality factor improvement by increasing copper thickness is limited by skin effect especially above 1 GHz. And reducing magnetic film thickness can improve both quality factor and frequency response at the expense of loosing inductance increase which indicates an optimized thickness for a magnetic thin film with certain permeability. Moreover, patterning magnetic film into finger and ring structure to reduce eddy current is also clearly shown in simulations.

A 4-turn rectangular sub-100μm spiral inductor is designed in HFSS (see Fig. 6) based on which all the simulations are set up. The magnetic thin film material here in simulations is modeled as Co-Zr-Ta-B (CZTB) which has a constant permeability of 1070 and conductivity of $8.7\times10^5$ siemens/m. The material properties used in the simulation are listed in Table IV while the dimensions of the spiral are in Table V.

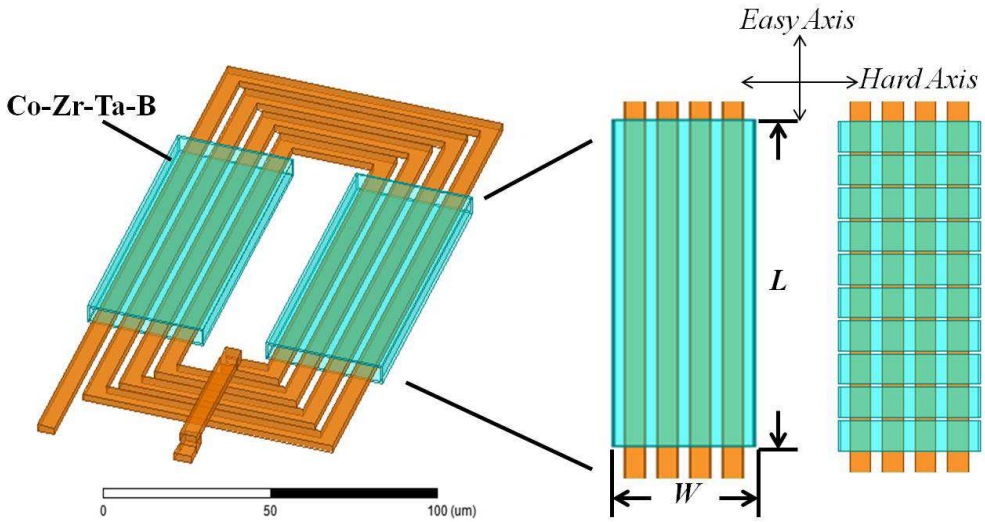


Fig. 6 Schematic of on-chip spiral inductor with Co-Zr-Ta-B magnetic thin film. Right: Top-view of un-patterned and patterned films (10 bars) with easy axis oriented along the copper coils.

Table IV. Material Properties in HFSS simulations

| | Conductivity σ (simens/m) | Relative Permittivity | Relative Permeability |
|---|---|---|---|
| Co-Zr-Ta-B | 870000 | 1 | 1070 |
| Polyimide | 0 | 3.5 | 1 |
| Substrates | 3.33 | 11.9 | 1 |

Table V. Dimensions of spiral inductors in HFSS simulations (μm)

| Outer diameter | Coils width | Coils space | turns |
|---|---|---|---|
| 160×88 | 5 | 3.5 | 4 |

### 3.1 Air-core Inductor Optimization

The series resistance of inductor is calculated by Eq. (2) which determines the quality factor.

$$R_s = \frac{\rho \cdot \ell}{W \cdot \delta \cdot \left(1 - e^{-t/\delta}\right)} \tag{2}$$

Where δ is skin depth given by

$$\delta = \sqrt{\frac{\rho}{\pi \mu f}} \tag{3}$$

Eq. (2) shows that skin depth is frequency dependent parameter and for copper at 1 GHz, the skin depth is about 2 μm. Simulated copper thickness is ranging from 2 μm to 7 μm selected according to the fabrication capability. Fig. 7 shows that increasing copper thickness can help improve quality factor below 1 GHz, however, over 1 GHz such improvement becomes trivial.

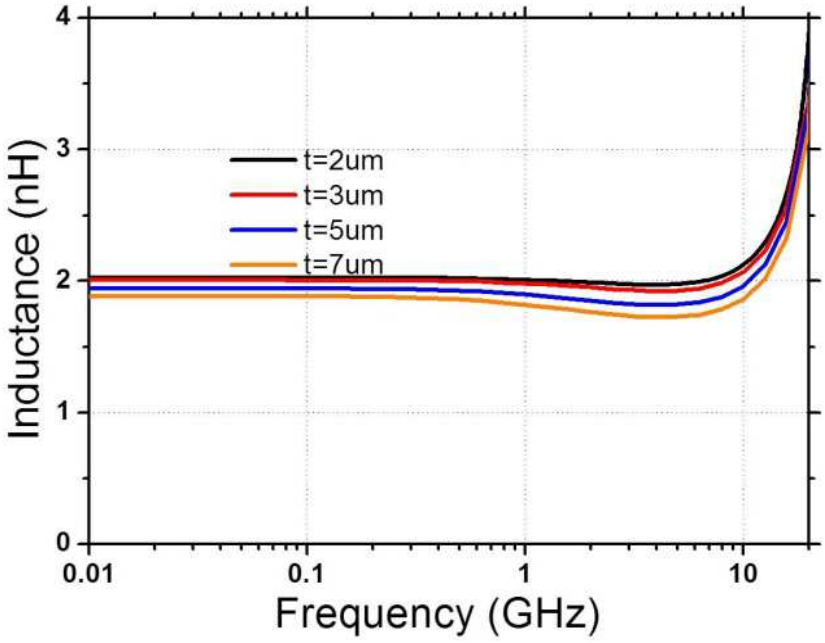

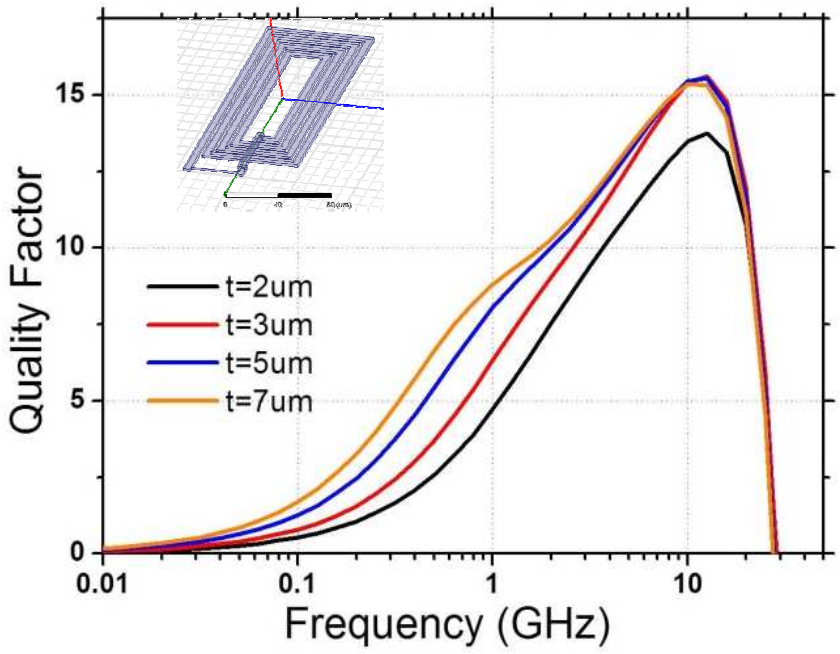


Fig. 7 Simulations with different copper coil thickness. Thickness is ranging from 2μm to 7μm. Inset shows the structure of simulated air-core spiral inductor.

### 3.2 Magnetic Film Thickness Optimization

The thickness of magnetic film determines the amount of magnetic flux increase in total. The thicker the magnetic film is, the more increase in magnetic flux. But as the flux increases, induced eddy current in magnetic film is also increasing. Simulations on different magnetic film thickness are helpful to choose appropriate film thickness for different applications. Fig. 8 is the simulation result showing that the magnetic film should keep less than 1 μm thick otherwise the eddy current loss will be so large that inductance and quality factor drop a lot even at MHz range. Though the FMR effect is not accounted here, it still shows that only films thinner than 500 nm are suitable for GHz applications.

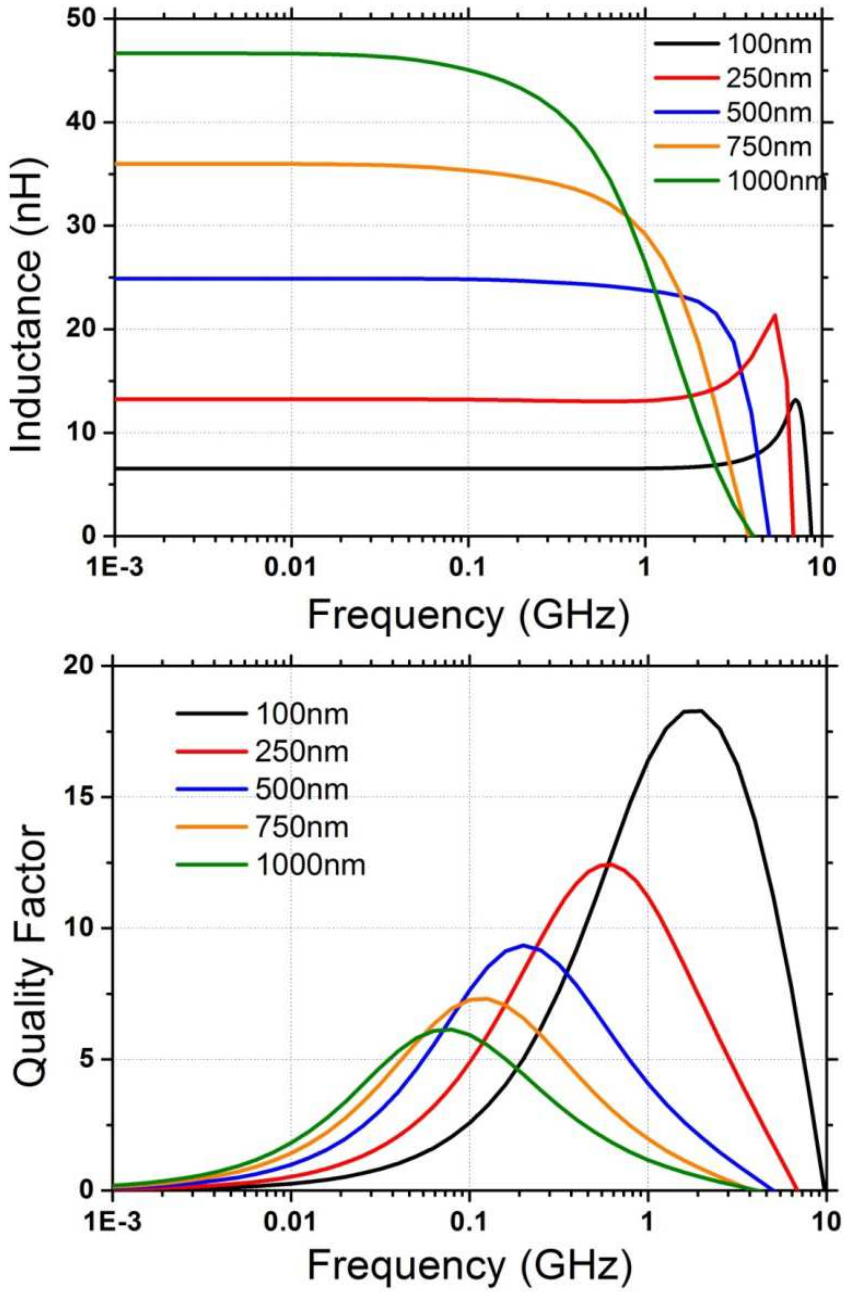


Fig. 8 Simulations with different magnetic thin film thickness. The thickness limit is about 1 μm which is determined by eddy current loss in the magnetic film.

### 3.3 Magnetic Film Structure Optimization

Eddy current in magnetic films is induced by the magnetic flux generated by copper coils. The magnetic via regions where top and bottom layer of magnetic film connect to

each other (as shown in Fig. 10) usually have the most strong magnetic flux penetrating. Therefore, large amount of loss is generated in magnetic via regions. As seen in Fig. 10, the current density is very high in conventional magnetic vias. Patterning these magnetic vias can effectively reduce the eddy current so that quality factor can be improved. In HFSS, so-called fingers structure is designed and simulated shown in Fig. 9. The frequency response has been improved from 1 GHz to about 2~3 GHz and the quality factor increases more than 30%. However, this method has its limit when fingers number is more than 12 demonstrated by simulations.

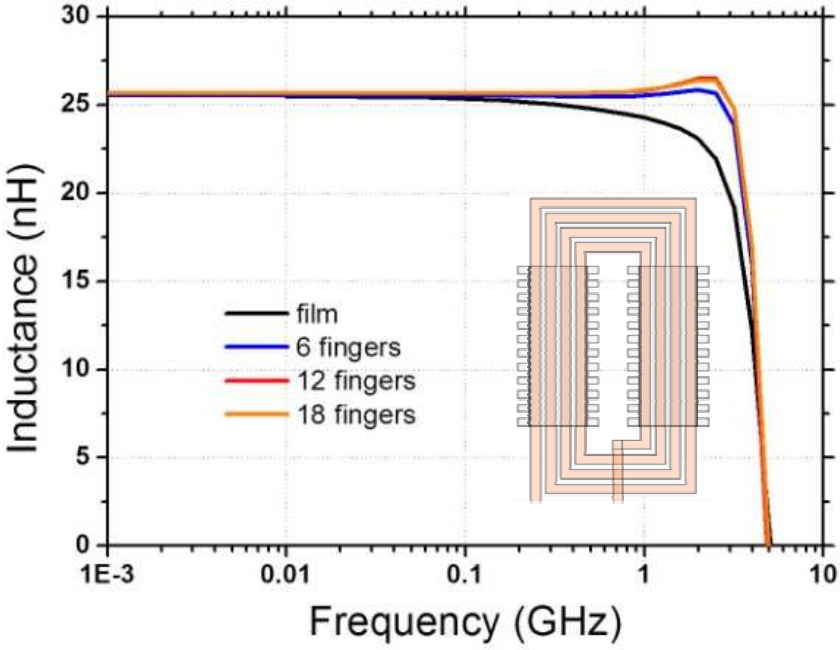

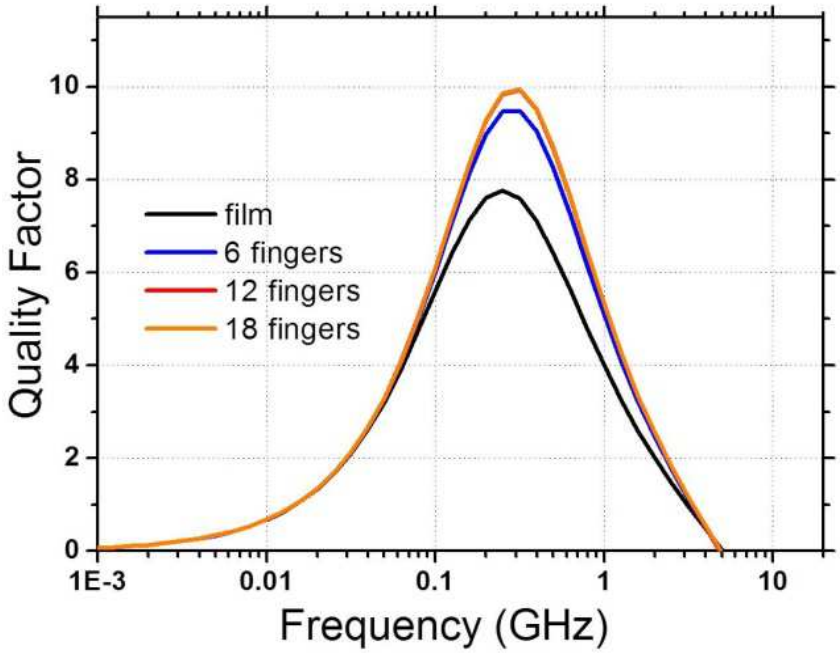


Fig. 9 Simulations on patterned magnetic vias. Schematic of finger structure is shown in the inset. The curves of 12 fingers and 18 fingers are overlaid which means patterning would not continuously improve the inductor performance after cutting into very fine fingers.

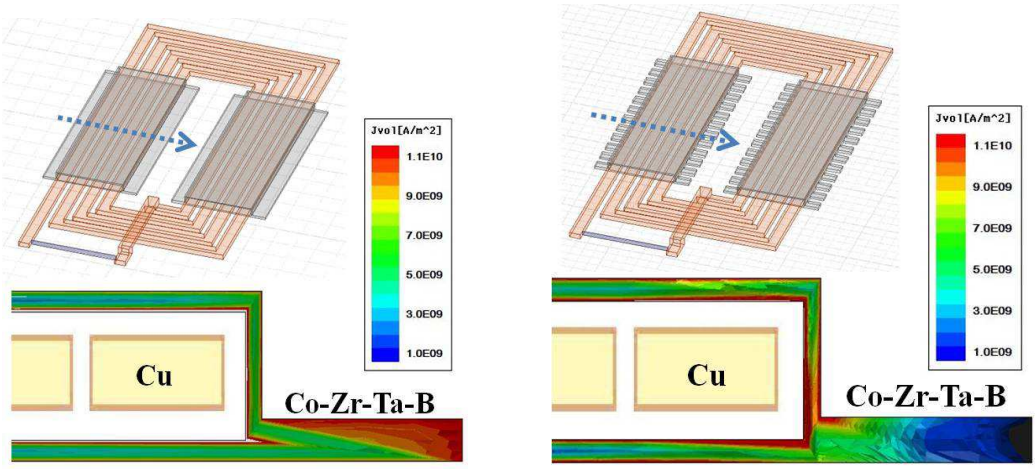


Fig. 10 Simulations of current density (at 1GHz) in magnetic films without (left) and with (right) finger-shaped magnetic vias from ANSYS HFSS 3D EM simulator. Current density was shown in cross-sectional view and the arrows in the top-view showed the direction and position of the cross-sectional view.

Different from finger structure in which only magnetic via regions are patterned slotting structure has the complete magnetic films cut into rings, shown in Fig. 11. The

idea is to cut the eddy current loop in the magnetic films. From the simulation results shown in Fig. 11, the improvement is only observed in 40 and 80 ring structure which means eddy current does not form large loop in magnetic thin film. This method is not an effective way to suppress eddy current loss. However, HFSS simulation cannot calculate magnetic properties changes when magnetic film turns into narrow rings. From material point of view, this patterning is useful to increase the anisotropy field in the film resulting in higher FMR.

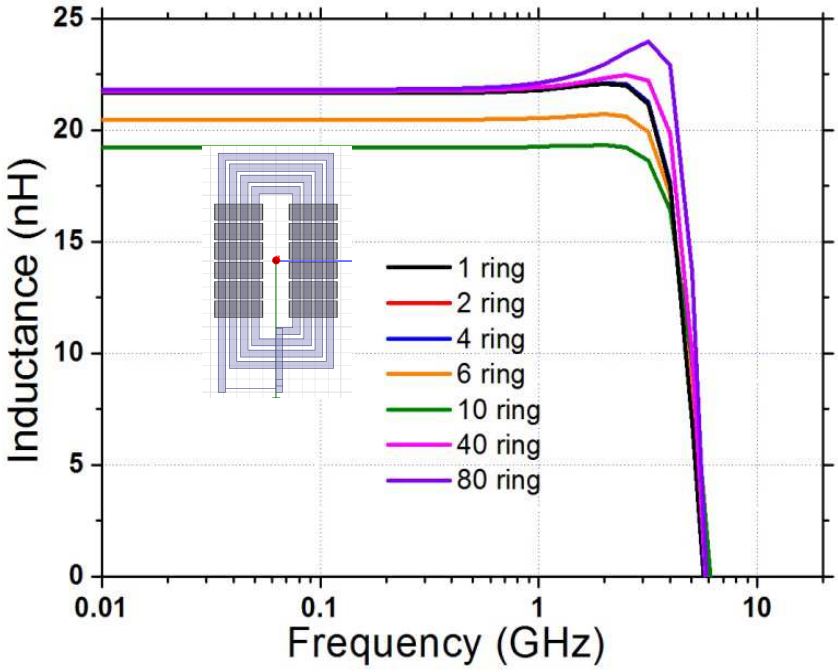

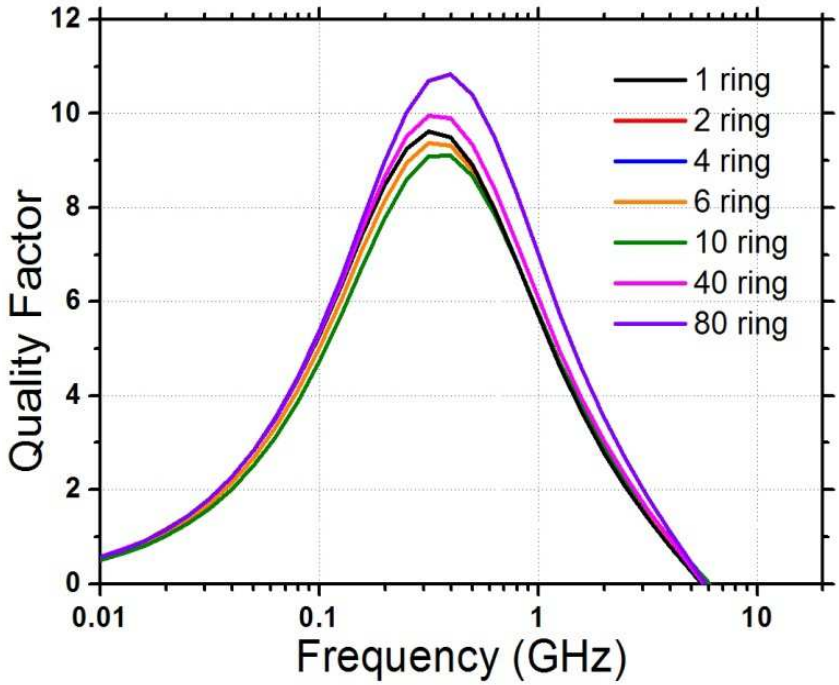


Fig. 11 Simulations on patterned magnetic films. Inset shows an example of 6-ring structure. The improvement can be seen after the magnetic film is cut into very small rings.

### 3.4 Conclusion

To summarize all the simulations in HFSS, it is demonstrated

(1) Increasing copper thickness only improves low frequency quality factor. At high frequency range (above 1 GHz) the skin effect limits the quality factor improvement. The optimized copper thickness can be chosen from 2μm to 5μm for future fabricated device.

(2) Magnetic film thickness has strong effects on both inductance and quality factor. There is a trade-off between inductance increase and peak quality factor. Thinner magnetic film has lower inductance increase but large peak quality factor at higher frequency. The simulations indicate that magnetic film below 500 nm is suitable for RF applications.

(3) Finger structure is useful to improve inductor’s performance; however, there is no need to pattern magnetic vias into very fine finger structure according to simulation results.

(4) Eddy current cannot be effectively suppressed by patterning the magnetic film into rings structure. Only when the rings are very small can quality factor improvement be seen.

# Chapter 4

# ON-CHIP INDUCTORS WITH LAMINATED AND MICRO-PATTERNED CO-ZR-TA-B MAGNETIC THIN FILMS

In this chapter, boron-incorporated amorphous Co-Zr-Ta-B films with high resistivity are integrated into on-chip inductors to achieve up to 9.1X inductance increase with good frequency response up to 2 GHz. It is demonstrated that laminations can suppress the eddy current loss in magnetic films resulting in better frequency performance. Effects of patterning magnetic film have also been investigated by changing magnetic thin film aspect ratio. It was demonstrated that the peak Q can be pushed towards high frequency as far as 1GHz by a combination of patterning magnetic films into fine bars and laminations.

## 4.1 Inductor Fabrication

Spiral and stripe inductors were fabricated onto quartz substrates using electron beam lithography (EBL) and magnetron sputtering for pattern definition and metallization, respectively. The spiral inductors are 4-turn rectangular-shaped with outer diameters of 88 μm by 160 μm and an inductance of 1.9 nH without magnetic material. Copper wires are 2 μm thick and 5 μm wide wrapped around by Co-Zr-Ta-B thin films (see Fig. 6). Polyimide was used as insulating layers separating the copper conductor and the magnetic material. The amorphous Co-4%Zr-4%Ta-8%B (at.%) alloy was prepared by DC magnetron sputter deposition. Material preparation and characterization are discussed in section 2.3. Besides spiral inductors, 450 μm-long stripe inductors were also fabricated with both laminated and non-laminated films. Two layers of Co-Zr-Ta-B films were integrated into both spiral and stripe inductors by joining the two layers through

magnetic vias to form a continuous magnetic circuit for maximum flux enhancement. The thickness for each layer is 500 nm determined by the skin depth of magnetic material at GHz frequency range.[50] Thicker films will induce larger eddy currents that will deteriorate the quality factor. Various magnetic film structures were fabricated to obtain a comprehensive understanding. HP8720D network analyzer and Cascade GS probes were utilized for one-port measurements.

**4.2 Stripline Inductors with Laminated Co-Zr-Ta-B Films**

To reduce the eddy current and skin effect, Co-Zr-Ta-B films were laminated using five 100nm layers separated by cobalt oxide so that the total magnetic film thickness remains 500nm for comparisons. 450μm-long stripe inductors were fabricated with 500nm thick both laminated and non-laminated films. A maximum inductance increase of 9.1X was achieved in stripe inductors with laminated Co-Zr-Ta-B films whereas only 4X inductance increase was measured from non-laminated films, shown in Fig. 12. This large inductance increase from laminated films is partially due to mitigation of skin effect in magnetic films. Also, laminations help suppress the strip/vortex domains which deteriorate permeability of magnetic film. [42]

Furthermore, maximum quality factor was nearly 3 but started to roll-off above 300MHz. As discussed before, the losses in the magnetic films due to eddy current and FMR are always coupled. However, the roll-off observed in quality factor of stripe inductors mainly comes from FMR which is determined by the Kittel equation [40] as

$$f_r = \frac{\gamma}{2\pi}\sqrt{\frac{M_s H_{eff}}{\mu_0}} \tag{4}$$

$H_{eff}$ is the effective anisotropy field given by

$$H_{eff} = H_k + N_d M_s \tag{5}$$

The second term in Eq. (5) is shape anisotropy filed where $N_d$ is the demagnetizing factor controlled by patterning the magnetic films. High shape anisotropy field will increase the FMR frequency. However, there is a tradeoff between FMR frequency and low-frequency permeability since the effective permeability is defined as

$$\mu_{eff} = \frac{M_s}{H_{eff}} = \frac{M_s}{H_k + N_d M_s} \tag{6}$$

Therefore, introducing high shape anisotropy into magnetic thin film would help push the FMR frequency high enough above the operating frequency with the drawback of a proportionally reduced permeability. From the experiments, the laminated magnetic films were patterned into 25μm-long and 10μm-wide bars resulting in better high frequency response but lower inductance increase, as seen in Fig. 12.

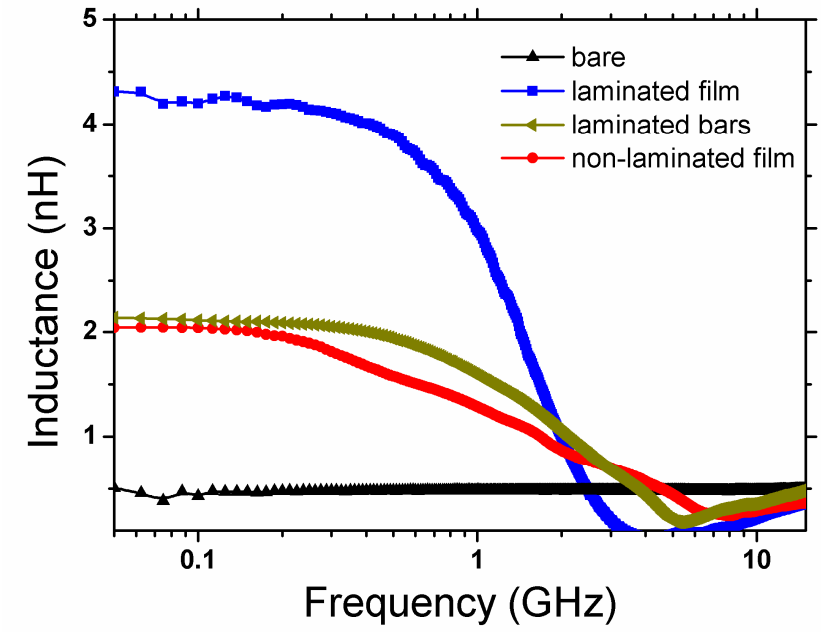


(a)

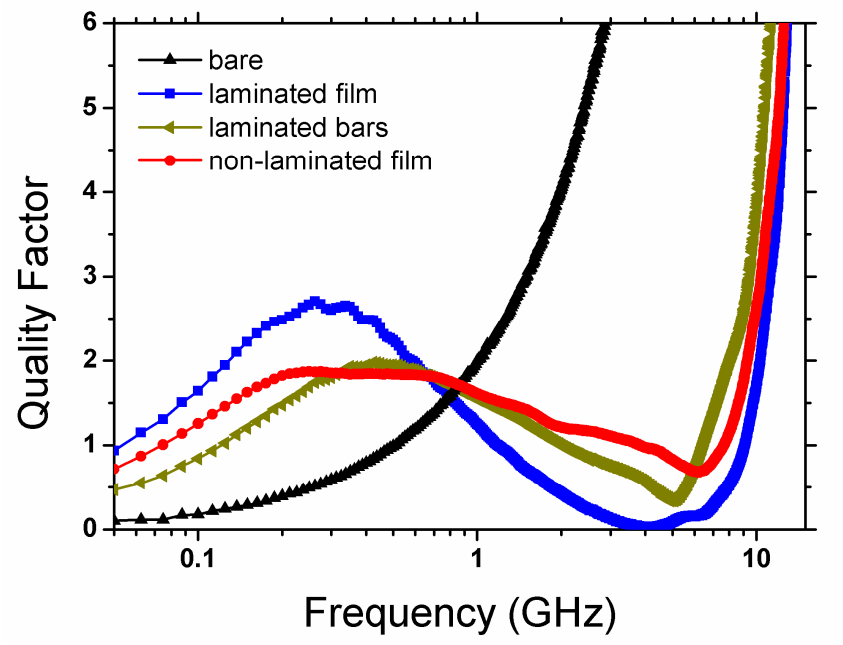


(b)

Fig. 12 Inductance (a) and quality factor (b) measurements from stripline inductors with 5×100nm laminated versus non-laminated Co-Zr-Ta-B films. The "bare" represents the same inductor without magnetic materials.

**4.3 Spiral Inductors with Laminated Co-Zr-Ta-B Films**

Measurements of inductance and quality factor versus frequency of spiral inductors using three combinations of laminations and non-laminated single layer film are shown in Fig. 13. Notable improvement in high frequency response (100 MHz to 1 GHz) was observed from the inductors with laminated films. With 500 nm thick non-laminated film the inductance increases by 3.4 times whereas a 30% more inductance increase is obtained using laminated films. Besides, comparing the slopes of inductance versus frequency curves one notes that inductance drops faster for non-laminated films as frequency increases. This frequency dependent inductance drop is due to the skin depth effect that the field cannot penetrate evenly in the magnetic films resulting in a lower effective permeability. Reference [51] gives a theoretical method to calculate this

effective permeability considering skin depth effect. However, the inductors with 10 layers of laminations show a slight inductance drop at low frequency which arises from the added reluctance from the laminations in the magnetic vias. [52]

Another advantage of using laminations is to suppress eddy current loss in the conductive magnetic films. By laminations the peak quality factor has been improve more than 50% from 1.5 of non-laminated film to 2.4 of 10 laminations film. The peak quality factor of 2.4 appears at 500MHz making the on-chip inductor suitable for RF applications.

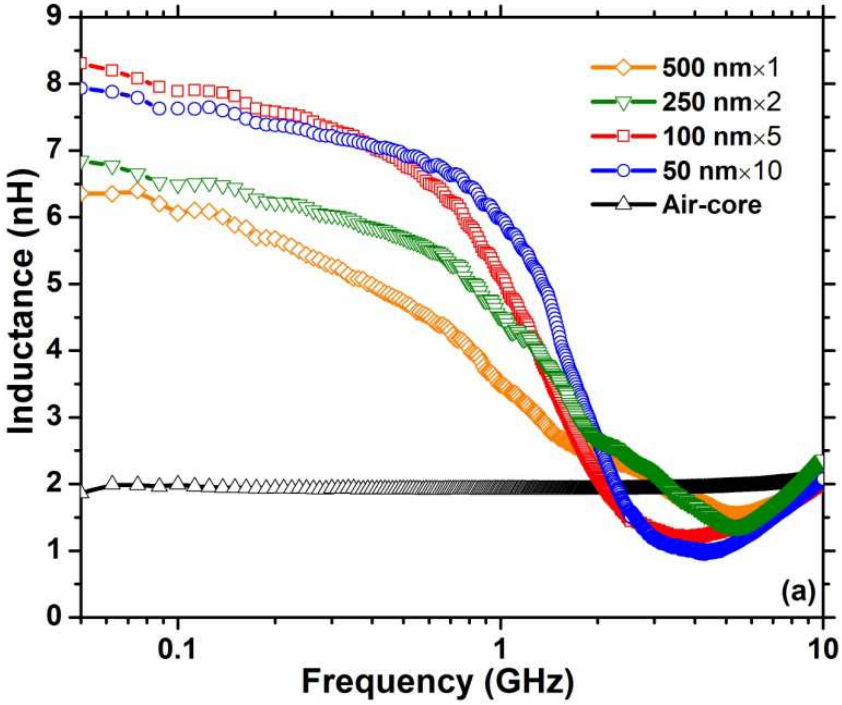

(a)

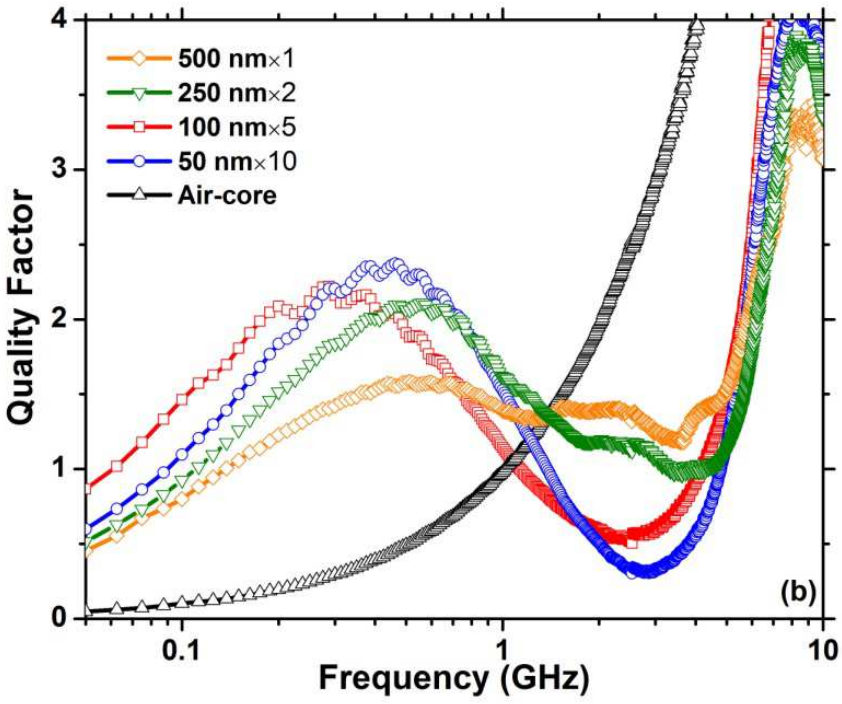


(b)

Fig. 13 Measurements of (a) inductance and (b) quality factor of spiral inductors with laminated Co-Zr-Ta-B films.

To further improve on-chip inductors high frequency performance, the laminated Co-Zr-Ta-B film was patterned into small bars while the film width and total length were kept the same, see Fig. 6. This patterning technique is sometimes also termed slotting, which introduces slots in the continuous magnetic film in the direction perpendicular to the inductor wire with an intention to cut off eddy current flow in the magnetic film that has a direction that counters the current flow in the inductor wire. Measurements results in Fig. 14(a) show that the inductance drops as magnetic films turn into small bars. There are several factors that could lead to the inductance decrease in patterned films. One factor is the filling ratio of patterned films defined as the bars length divided by the sum of bars length and gap distance between bars. The smaller the filling ratio is, the less

magnetic material in the core, thus leading to less flux augmentation. Table VI shows the filling ratio in comparison to the inductance increase change. Apparently there is no linear relationship between filling ratio and inductance increase change; however, for 4 bars and 6 bars these two parameters are very close whereas beyond that the inductance drops more rapidly than filling ratio, as in the case of 10 bars. This indicates that as patterning magnetic film into small bars with large aspect ratio (L/W) the effect of shape anisotropy comes in and becomes the dominant factor over filling ratio. Large shape anisotropy field contributes to the effective anisotropy field resulting in a decrease in effective permeability. [53]

Table VI. Effect of patterning on inductance increase change

| | Film | 4 bars | 6 bars | 10 bars |
|---|---|---|---|---|
| Aspect ratio (L/W) | 1/0.5 | 1/3 | 1/5 | 1/10 |
| Filling ratio | 100% | 82% | 68% | 57% |
| Inductance increase change | 100% | 86.4% | 68.6% | 45.5% |

The quality factor curves in Fig. 14(b) present a right shift towards higher frequency with increasing patterned bars. Therefore, at low frequency range inductors with patterned magnetic bars show a lower Q factor while a contrasting trend occurs at high frequency range. Fig. 15 shows the effect of patterning on the peak Q value and position in frequency domain. A peak Q of nearly 3 is achieved by the smallest bars (10 bars) at about 1 GHz. With fine patterning peak Q goes towards up-right corner of this plot where large Q appears at high frequency. This demonstrates that patterning film into bars structure is helpful in reducing eddy current loss in the inductor and is necessary for obtaining high Q factor in a high frequency range.

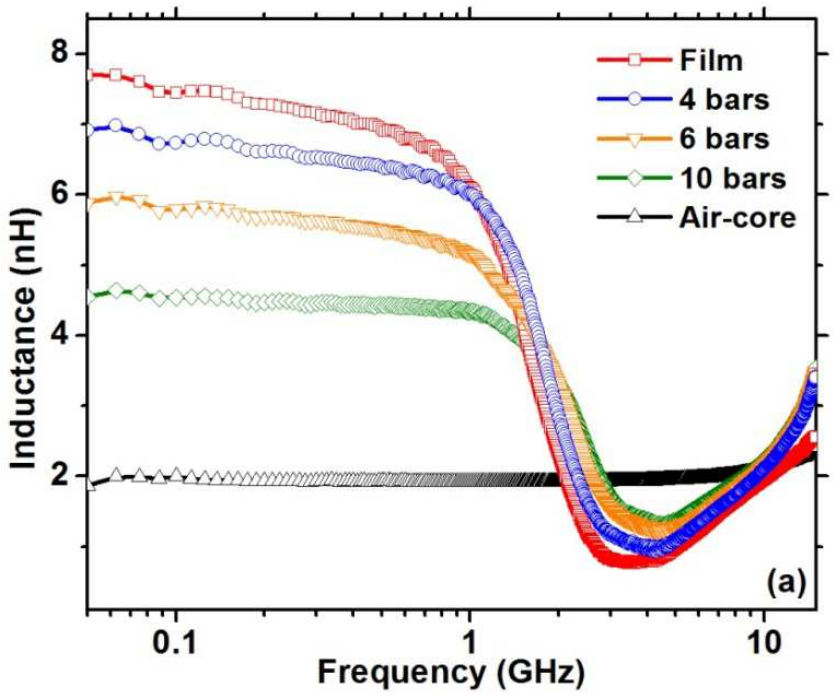


(a)

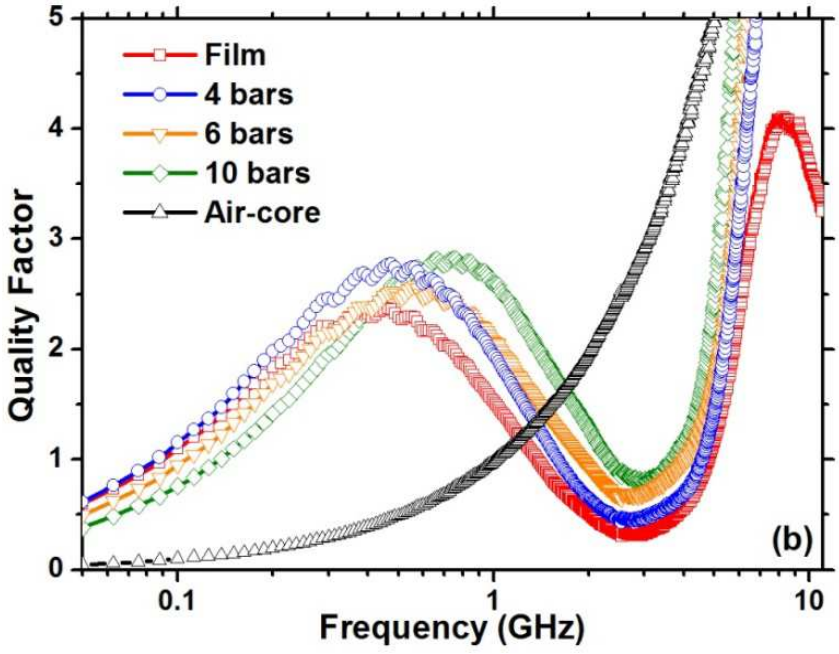


(b)

Fig. 14 Measurements of (a) inductance and (b) quality factor of spiral inductors with patterned Co-Zr-Ta-B films.

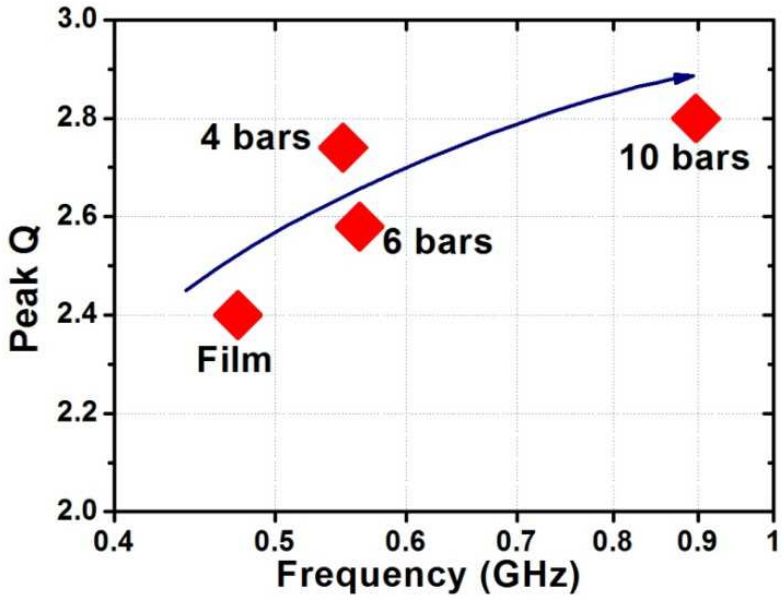


Fig. 15 Effect of patterning on the peak Q value and position in frequency domain. The arrow indicates that with fine patterning peak Q goes towards up-right corner of this plot.

## Chapter 5

## CONTROL OF MAGNETIC FLUX AND EDDY CURRENT IN MAGNETIC FILMS IN ON-CHIP RADIO FREQUENCY (RF) INDUCTORS

In this chapter, the role of magnetic vias in magnetic flux and eddy current control is investigated by both simulation and experiment using different patterning techniques and by altering the magnetic via width. Improved finger-shaped magnetic vias have been designed and integrated into on-chip RF inductors improving the frequency of peak quality factor from 400 MHz to 800 MHz without sacrificing inductance enhancement. Eddy current and magnetic flux density in different areas of magnetic vias are analyzed by HFSS 3D EM simulation. With optimized magnetic vias, high frequency response of up to 2 GHz has been achieved.

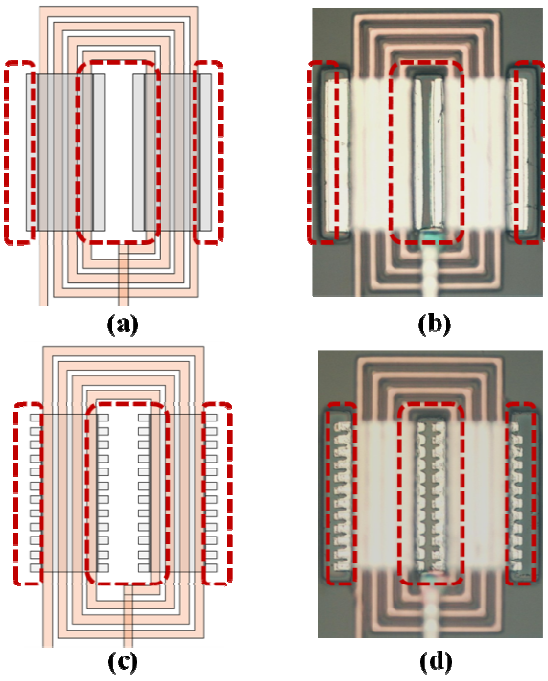


Fig. 16 Top-view of schematic and fabricated 4-turn spiral inductors with regular (a) (b) and finger-shaped (c) (d) magnetic vias. Cu coils were wrapped around by Co-Zr-Ta-B, and the dashed lines indicated magnetic via regions.

### 5.1 Spiral Inductors with Finger-shaped Magnetic Vias

The spiral inductors were elongated to take advantage of the uniaxial magnetic anisotropy and the Co-Zr-Ta-B films were patterned for optimizing the spiral inductors performance, as shown in Fig. 16.

Fig. 17 presents measured inductance (L) and quality factor (Q) for 4-turn rectangular inductors with different magnetic thin film structures. Compared to inductors without magnetic films (bare in Fig. 3), a 4-turn rectangular spiral inductor with a single magnetic ring achieved a maximum 3.5X inductance increase and a 3.9X increase in the Q-factor at 1 GHz.

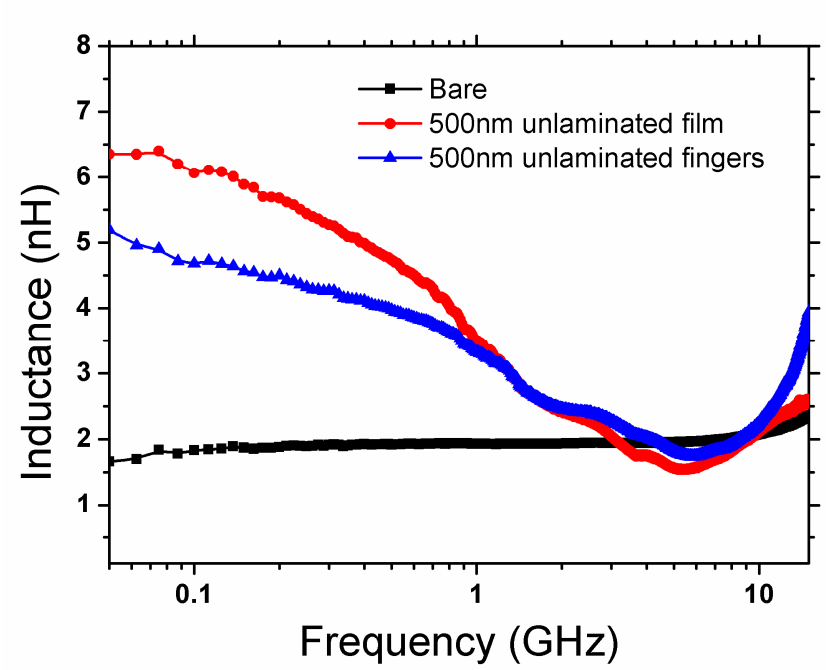


(a)

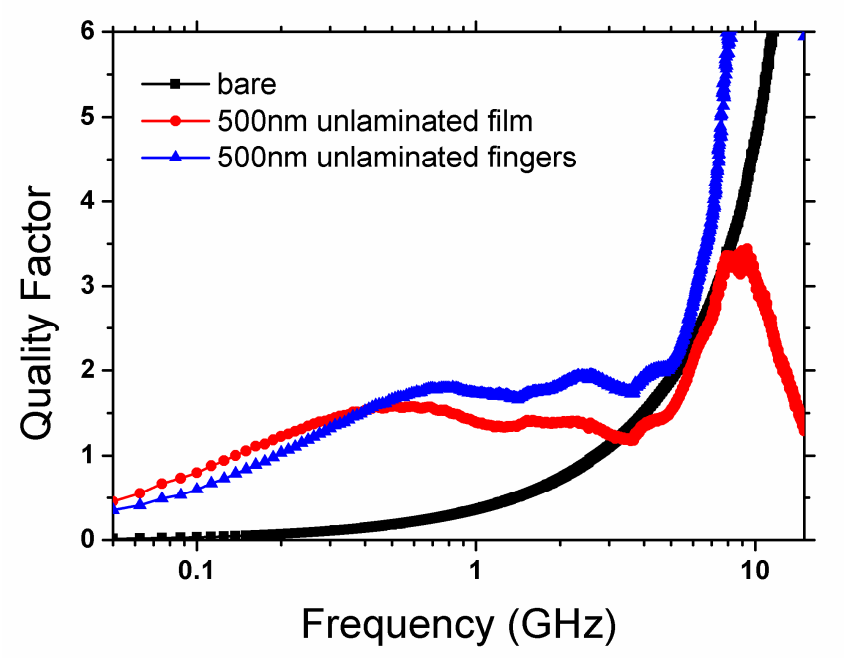


(b)

Fig. 17 Inductance (a) and quality factor (b) measurements from 4-turn rectangular spiral inductors with regular and finger-shaped magnetic vias. The Co-Zr-Ta-B film is 500nm thick without laminations. The "bare" represents the same inductor without magnetic materials.

The inductance begins to drop dramatically above 1 GHz from various sources of magnetic loss, e.g., eddy currents in the magnetic material, skin effect and FMR effect. As a result, quality factor does not continue increasing above several hundreds of MHz until resonant frequency is reached. ANSYS HFSS was used to simulate the eddy current distribution in the magnetic films. The volume current density plotted in Fig. 18 has shown that the strongest eddy current density appears in the magnetic via regions. Minimizing the size of magnetic vias is therefore one efficient way to suppress the eddy currents. Finger-shaped magnetic vias have been designed to cut off the eddy current loop in magnetic vias whereas keeping the magnetic flux continuous. Simulations show the current density in finger-shaped magnetic vias decreases over one-order. This is proved

by experiment results, as seen in Fig. 17, the inductors with finger-shaped magnetic vias have better frequency response and higher high-frequency quality factor.

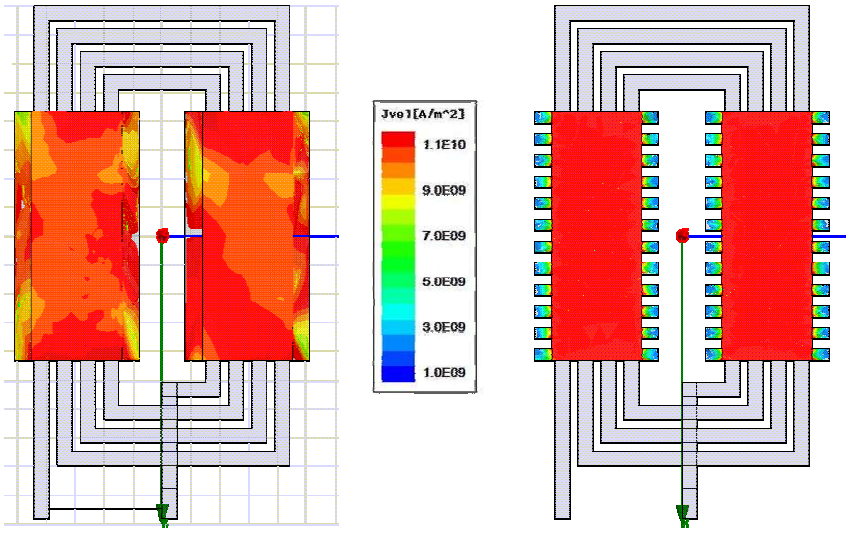


(a) (b)

Fig. 18 Simulations of current density (at 1GHz) in magnetic films without (a) and with (b) finger-shaped magnetic vias from ANSYS HFSS 3D EM simulator.

The reason for this decrease is that the sidewall of the magnetic via was also patterned along with the finger structure where magnetic flux was no longer continuous along the entire magnetic vias. In order to maintain inductance value, improved finger-shaped magnetic vias shown in Fig. 19 were designed in which only the extension portion (see Fig. 19 (b) and (c)) was patterned into finger shape while keeping the sidewall continuous along the entire magnetic via. Fingers are patterned with different length, 12 μm, 4 μm, 2 μm for 6 fingers, 12 fingers and 20 fingers, respectively. Fig. 20 shows the frequency dependence of measured inductance (L) and quality factor (Q) from inductors with regular and improved finger-shaped magnetic vias. Even though magnetic vias were partitioned into small fingers that has less magnetic materials, the inductance still maintains near constant value and high compared to that of regular inductor without

fingered structure, whereas peak quality factor has improved from 400 MHz to 800 MHz compared to the latter. The demonstrated high frequency peak quality factor is a result of the suppression of eddy current loss by the finger structure in the extension portion of magnetic vias, and was demonstrated earlier by HFSS simulation.

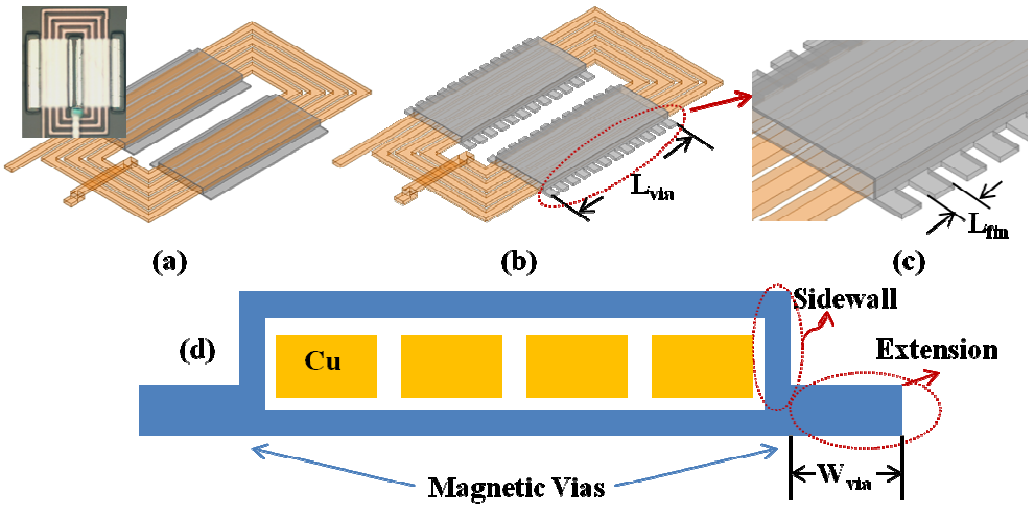


Fig. 19 (a) Schematic and fabricated (inset) on-chip magnetic thin film spiral inductor with regular magnetic vias. (b) Schematic of improved finger-shaped magnetic vias with 12 fingers (c) Zoom in improved finger-shaped magnetic vias showing fingers length and width. (d) Cross sectional view of magnetic vias composed of sidewall and extension portion.

In addition, the peak quality factor did not show more significant improvement when magnetic vias have more fingers (from 2.2 for 6 fingers to 2.5 for 20 fingers). From this observation, it is suggested that if one aims at maximizing the quality factor towards high frequency, the width of the extension portion need to be reduced as well. One disadvantage of reducing the extension width is the inductance drop. However, according to the measurement results in Fig. 20, when magnetic vias were patterned from regular shape to fingers with less magnetic materials the slightly changed inductance value indicated that the sidewall is more critical to inductance enhancement compared to the

extension. Fig. 21 shows the magnetic field H distribution around inductor coils simulated in HFSS. Magnetic vias have smaller magnetic field in their 1 μm thick extension portion because eddy current in this area screens the external magnetic field. On the other hand, it is clear to see that magnetic flux is in a continuous loop throughout the sidewall. Therefore, the main strategy for optimizing magnetic vias is to minimize the extension portion, which will be discussed in the next section, providing the sidewall remains the same.

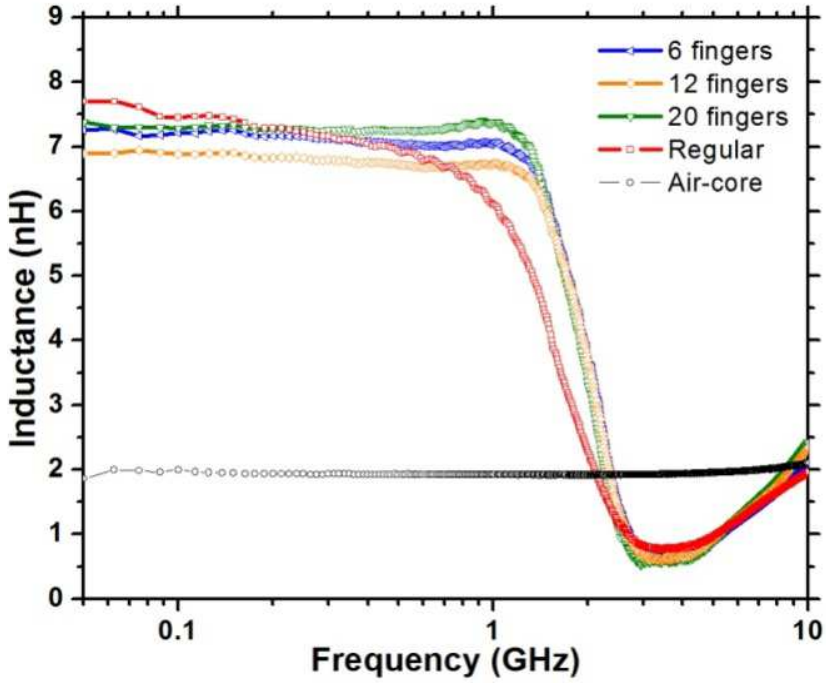


(a)

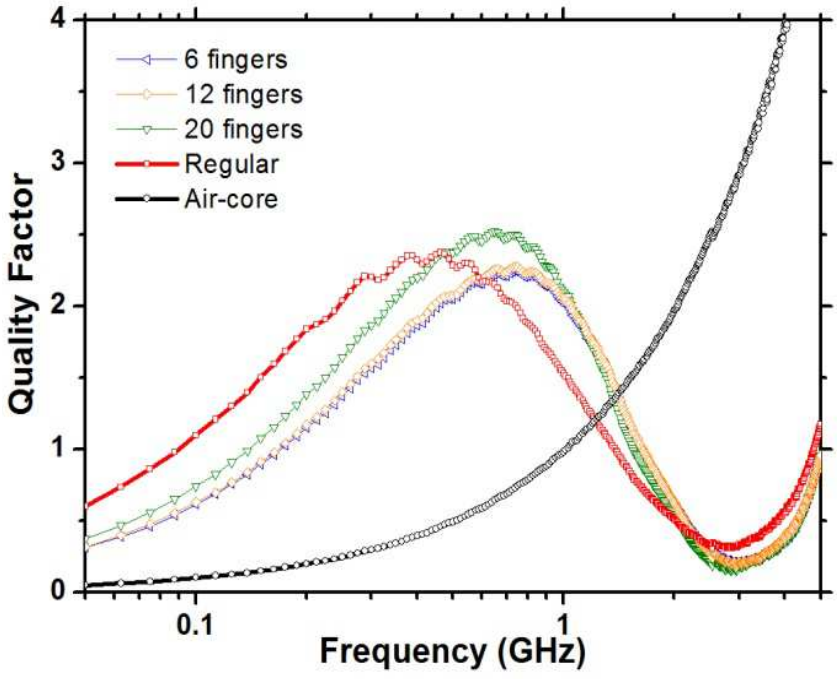


(b)

Fig. 20 Inductance (a) and quality factor (b) measurements from inductors with different magnetic vias.

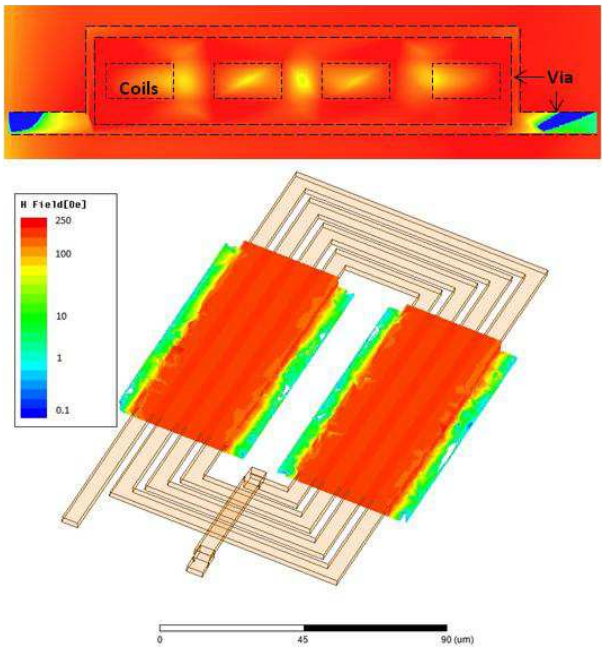


Fig. 21 Magnetic field in magnetic thin film around copper wires at frequency of 100 MHz showing that the extension portion of magnetic via actually does not contribute to the flux enhancement.

### 5.2 Width dependence of magnetic vias

In order to investigate roles of the sidewall and the extension of magnetic vias, further experiments were performed by altering the width of the extension portion of magnetic vias. First, inductors with magnetic vias consisting of only side wall were created in HFSS for simulation. It is as expected that the inductance has a similar value even though without the extension portion. In the fabrication process, however, the extension portion was intentionally kept to ensure good coverage of magnetic material on the sidewall during the sputtering process, as *Morrow et al.*[44] demonstrated that only approximately 25% of targeted magnetic material thickness on vertical sidewall can be achieved using sputtering deposition technique. The extension portion was altered from 1μm to 5μm. Measurement results showed that as the extension portion becomes narrower the inductor has a better high frequency response up to 2 GHz with a peak quality factor over 1 GHz, shown in Fig. 22. Meanwhile, the narrower magnetic vias lead to lower inductance value and for inductor with 1 μm wide magnetic vias the inductance drop by 40%, similar to what others have observed. [26, 44] This is due to the poor magnetic material coverage on the sidewall of magnetic vias. Fig. 23 shows the effect of extension portion width on inductance, peak quality factor and their related frequency. Although inductance increases as increasing the extension of magnetic vias, the peak Q does not follow this trend. More importantly, the frequency of peak Q and 90% L exhibit an opposite trend which means wide magnetic vias are not preferable in RF inductors. Future efforts to improve RF magnetic thin film inductors will focus on improving sidewall magnetic material coverage with minimum extension of magnetic vias.

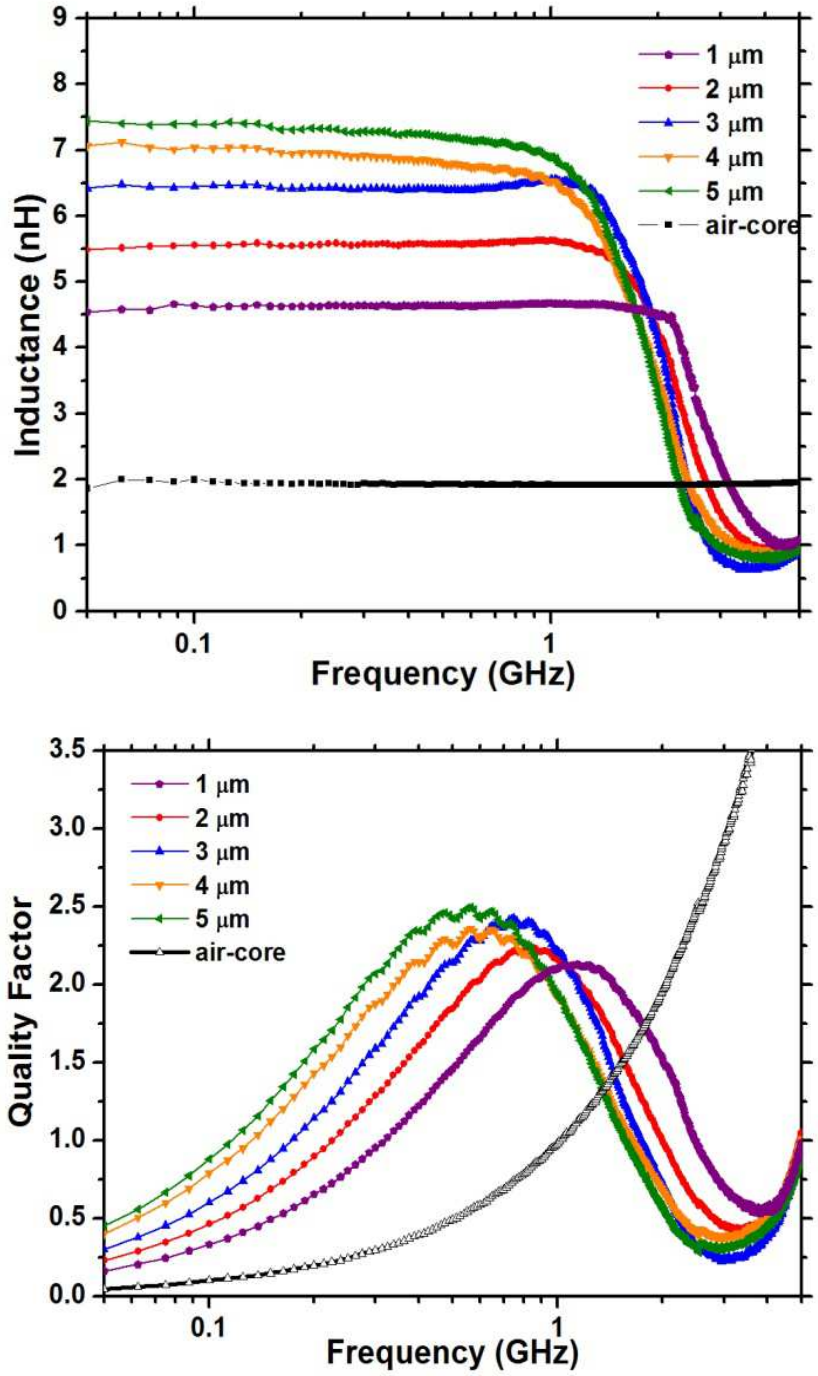


Fig. 22 Magnetic vias width dependence of inductance and quality factor of on-chip inductors. With narrow magnetic vias high frequency response up to 3 GHz and peak Q at 1.1 GHz can be achieved.

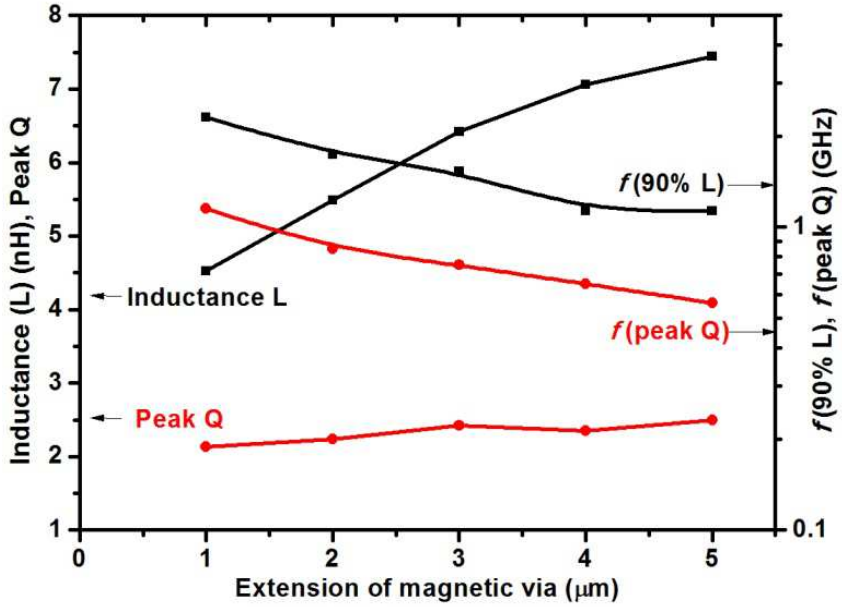


Fig. 23 Effect of extension portion width on inductance, peak quality factor and their related frequency, *f* (90% L) is defined as the frequency when inductance drops by 10%.

### 5.3 Summary

The magnetic via for controlling eddy current and magnetic flux is investigated to improve on-chip magnetic thin film inductors high frequency performance. Improved finger-shaped magnetic vias, which simultaneously suppresses eddy current and maintain magnetic flux loop, are helpful for achieving higher quality factor at higher frequency. The sidewall of magnetic vias is proven to play a critical role in forming magnetic flux path around inductor coils. By changing the extension of magnetic vias, magnetic via width dependence of L, peak Q and their frequency was examined showing that wide magnetic vias are not suitable for RF inductors.

# Chapter 6

# EFFECTS OF MAGNETIC FIELDS ON ON-CHIP INDUCTORS WITH PATTERNED MAGNETIC FILMS

Magnetic thin films are incorporated onto on-chip inductors to increase both inductance and quality factor making scaling down the on-chip inductors possible. These magnetic films properties are often obtained from flat, large area films. However, during device processing and patterning the magnetic properties can vary from flat films and therefore it needs a way to evaluate magnetic films in-situ after device fabrication. Some magnetic film properties, such as saturation magnetization, are also affected by device working conditions. In particular, in power management applications such as integrated voltage regulators utilizing magnetic film in the inductors, a high power density with large DC current will inevitably saturate the magnetic films resulting in the inductance decrease significantly thereby reduces the value of adding magnetic materials. Therefore it is crucial to quantify the saturation field in the fabricated inductor, as magnetic film in the inductor may not have the same saturation field as for large flat films where hysteresis loop and saturation field are typically obtained, and explore effect of various magnetic film structures that could increase the saturation field, therefore allowing larger current in the inductor coils for power delivery applications.

## 6.1 Experiment

The 4-turn spiral inductors were fabricated onto quartz substrates with 500-nm-thick amorphous Co-4%Zr-4%Ta -8%B (at. %) film prepared by DC magnetron sputtering. Fig. 24 shows the schematic (a) and fabricated devices with various patterned Co-Zr-Ta-B films including complete film (b), multiple bars (c) and film with finger-

shaped magnetic vias (d). HP8720D network analyzer and Cascade GS probes were utilized for one-port radio-frequency (RF) measurements. Inductors were tested by a small AC signal with a constant power of 5 dBm from 50 MHz up to 20 GHz. Meanwhile, a DC magnetic field generated by permanent magnets was applied perpendicular to the easy axis (EA) ranging from 0 Oe to 360 Oe as shown in Fig. 24.

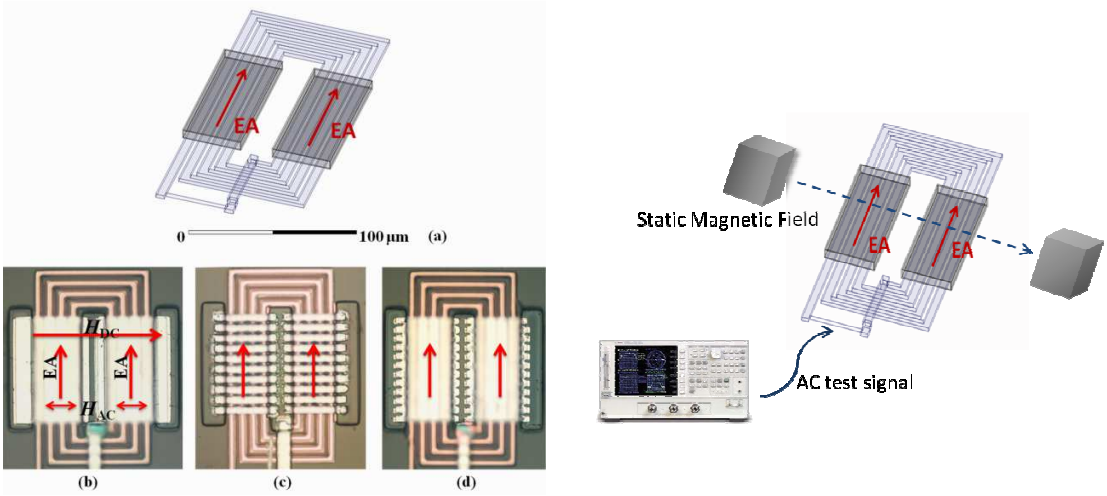


Fig. 24 Schematic (a) and fabricated (b-d) 4-turn spiral inductors with various patterned magnetic films, (b) film, (c) 10 bars, (d) fingers. Easy axis of magnetic film is indicated in each figure while both applied AC and DC magnetic field H are in the perpendicular direction.

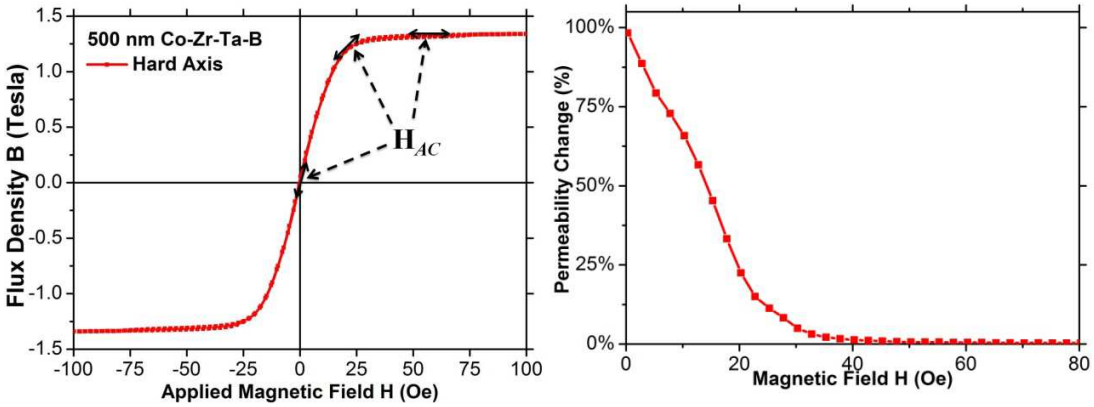


Fig. 25 (a) Measured hysteresis loops along Hard Axis (HA) of 500nm-thick large-area flat Co-Zr-Ta-B film. Arrows represent small AC signals under different DC biased magnetic field H. (b) shows the relative changes of the permeability

The hysteresis loop measured by vibrating sample magnetometer (VSM) from a 5 mm × 5 mm large area flat film on Si substrate is shown in Fig. 25 (a) indicating that the saturation field along hard axis (HA) is around 35 Oe. Magnetic material's permeability can then be calculated by taking the derivative of the B-H hysteresis loop. Due to the non-linear nature of the hysteresis loop, the permeability is variable with different applied bias field as seen in Fig. 25 (b), showing a maximum at zero bias and drops to 1 at 35 Oe bias field.

**6.2 Effects on Inductance and Quality Factor**

The low frequency inductance of an air-core planar spiral inductor can be calculated by simple approximate expressions which have very good accuracy. The calculated inductance of the air-core 4-turn inductor without magnetic materials is 1.9 nH which is validated by our measurement results. With magnetic material the inductance increases by a factor of $\mu_{eff}$, defined as effective permeability. $\mu_{eff}$ is determined not only by material intrinsic permeability but also geometric parameters such as magnetic film thickness and distance from inductor coils and fabrication process. Here we keep the process parameters all the same and apply a DC magnetic field along the hard axis while performing inductance measurement to render change of the magnetic states in the magnetic film around inductor coils. At low applied field from 0 Oe to 25 Oe the inductance versus frequency plots overlap with each other, indicating inductance and therefore magnetic film state remains unchanged for the entire frequency range, as shown in Fig. 26(a). As the applied H field continues to increase, however, the magnetic films on inductors gradually become deviated from initial state and inductance begins to drop at around 60 Oe and the trend continues until the magnetic film becomes fully saturated

and the effective permeability drops to 1. From the sequence of the field-dependent L measurement in Fig. 26(a), a saturation field of 220 Oe is determined when the magnetic film inductor has the same inductance value as the air-core one.

It should be noted that the 220 Oe saturation field for the magnetic film in the inductor structure here is much larger than the value of 35 Oe for an unpatterned flat film shown in Fig. 25 (b), due to the finite size and certain aspect ratio of the magnetic film in the inductor device structure that could alter the demagnetizing factor, leading to larger effective anisotropy field. More detailed discussion on demagnetizing factors is in Section B. This observation illustrates the importance of taking into account the magnetic film structure when saturation field is an important inductor design parameter.

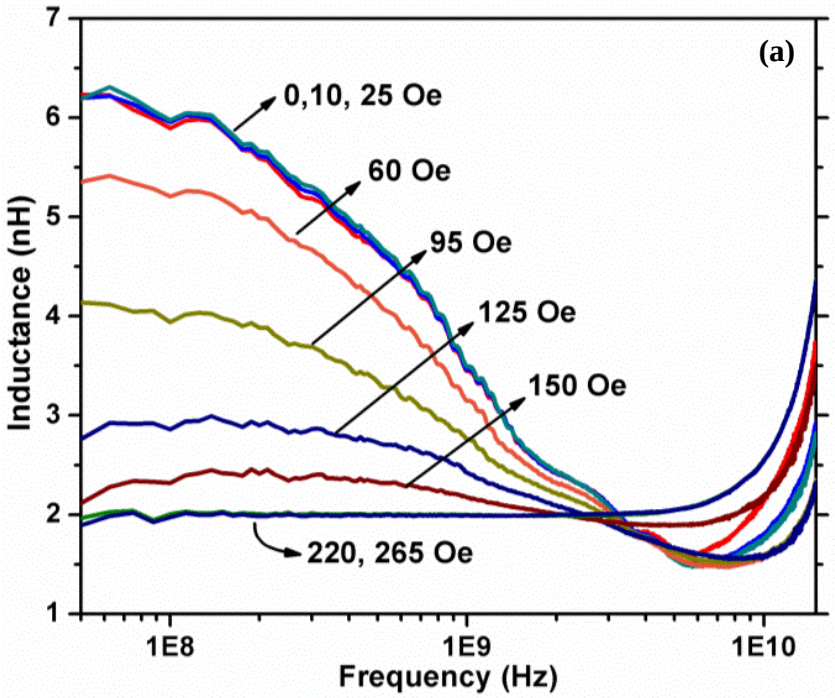

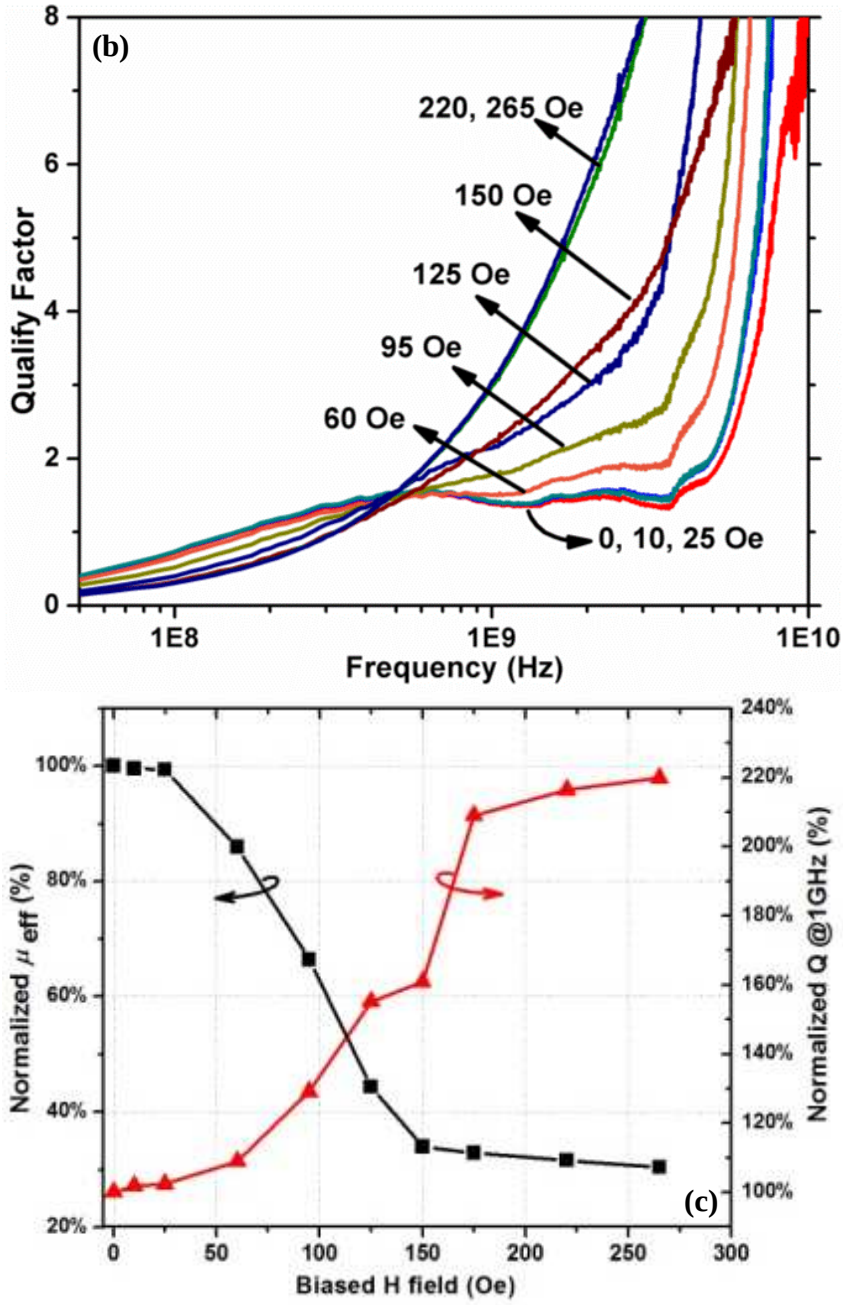


Fig. 26 Inductance (a) and quality factor (b) of 4-turn spiral inductor with complete Co-Zr-Ta-B film under different H field bias. Measurement was performed on device structure shown in Fig. 1(b), where magnetic layer is an un-patterned film. (c) Normalized effective permeability and quality factor at 1 GHz versus H field.

In addition, the quality factor at high frequency increases when high H field is applied. Without H field the quality factor plot versus frequency shows an obvious drop

at high frequency which is mainly due to the ferromagnetic resonant frequency (FMR) absorption. This FMR behavior is described by Landau Lifshitz equation:

$$\frac{dM}{dt} = -\gamma M \times H_{eff} + \lambda M \times (M \times H_{eff}) \tag{7}$$

where $\gamma$ denotes the gyromagnetic ratio and $\lambda$ is a damping parameter. The effective field $H_{eff}$ contains internal fields, the external bias field $H_{DC}$ and excited field $H_{AC}$. Under no bias field condition, the magnetization M is along the easy axis perpendicular to the excited AC field. So FMR absorption occurs at high frequency which is determined by Eq. (7). However, when external bias field applied to the hard axis, the magnetization M gradually becomes parallel to the $H_{eff}$ resulting in a zero curl product. The FMR effect is therefore minimized so that the quality factor remains large value at high frequency. Normalized effective permeability and quality factor at 1 GHz are plotted in Fig. 26(c) clearly showing these effects of external bias H field. After the magnetic film is saturated, the effective permeability is only 30% of its initial value whereas the quality factor increases by 220%.

**6.3 Patterned Magnetic Film**

The magnetic film is then patterned into various structures to investigate shape effects on the saturation field including bars (Fig. 24c) and finger (Fig. 24d) structures. The aspect ratio of magnetic film, defined as the length in hard axis direction divided by the length in easy axis direction, is used to distinguish these patterned films. From the measurement results in Fig. 27, which shows inductance versus applied filed at representative frequencies of 0.1 GHz and 0.5 GHz, it is obvious that, for magnetic film with large aspect ratio, the inductance drop to air-core value at smaller bias field.

Although for film, 2-bar and 4-bar structures there is little change in saturation, it reduces further for smaller bar width, such as 10-bar structure. This indicates there will be loss of magnetization with smaller width bars. Having lower saturation field in patterned bars is also due to the decreasing demagnetizing field $H_d$ which is calculated by (8).

$$H_d = -N_d M_s \tag{8}$$

$N_d$ is the demagnetizing factor along the hard axis calculated by the method discussed in chapter 2. With the demagnetizing field the effective saturation field becomes

$$H_{s,eff} = H_s + N_d M_s \tag{9}$$

As the aspect ratio increases, the demagnetizing factor along the hard axis decreases resulting in a decreasing saturation field. Table VII summarizes the patterned films' demagnetizing factors and corresponding calculated and measured effective saturation field. The discrepancy between calculated and measured saturation field is possibly due to the rough surface and uneven shape of the magnetic film deposited on fabricated devices.

Table VII Demagnetizing Factor and Saturation field of patterned CO-ZR-TA-B film

| | Film | 2 Bars | 4 Bars | 10 Bars | Fingers |
|---|---|---|---|---|---|
| Aspect ratio | 0.6 | 1.3 | 3.0 | 10.0 | NA |
| $N_d$ | 0.0178 | 0.0170 | 0.0147 | 0.0111 | NA |
| $H_d$ (Oe) | 258 | 248 | 219 | 175 | NA |
| $H_{sat}$ (Oe) | 220 | 220 | 220 | 150 | 325 |

On the contrary, the finger-shaped magnetic film has higher saturation field so that it can be used for large signal applications such as voltage regulators, especially at high frequencies. Comparing Fig. 27 (a) and (b), the trend that the finger-shaped film is less easy to be saturated is more distinct at high frequency range. For instance, at 0.1 GHz, the inductance of finger structure is slightly lower than that of inductor with film structure at field of 100 Oe in Fig. 27(a); its inductance is, however, higher than its film counterpart at 0.5 GHz at the same 100 Oe. This is consistent with our early observation that finger structure has better response and quality factor at higher frequencies. A possible explanation for high saturation field could be the edge-induced domains in the fingers structure that would require higher field to alter the magnetization direction, which requires further investigation.

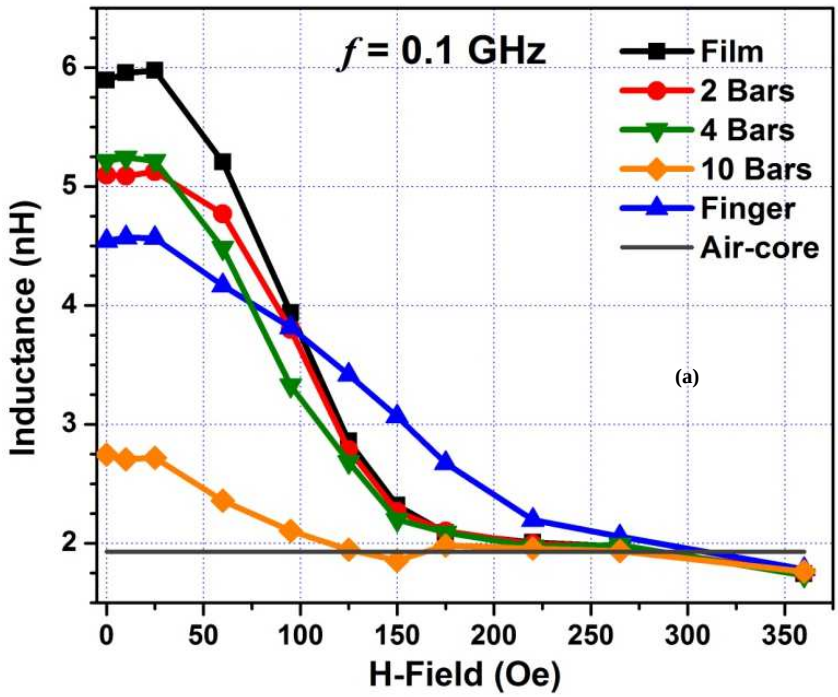


(a)

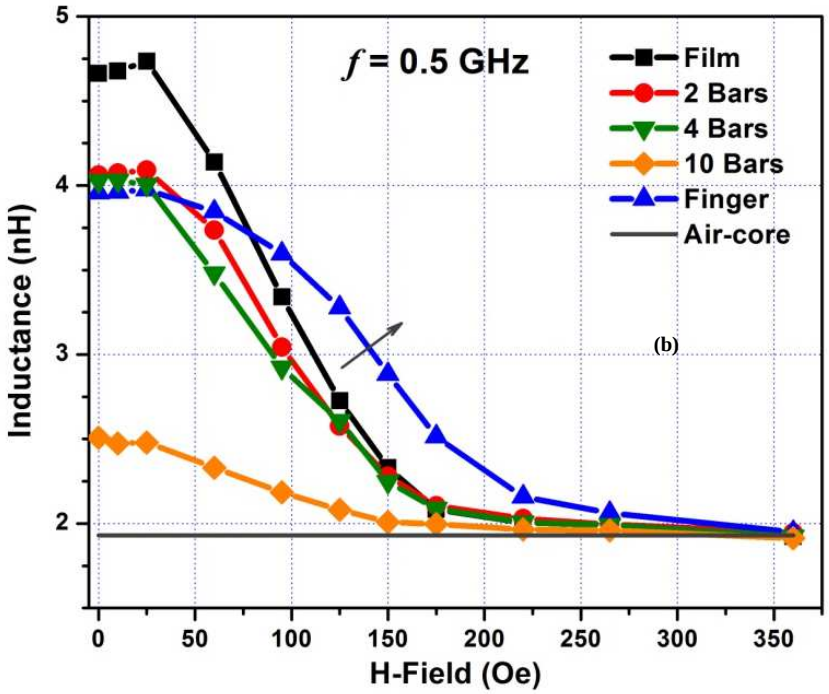


(b)

Fig. 27 Comparison of inductance versus bias field measured from inductors with un-patterned and patterned magnetic films at (a) 0.1GHz, (b) 0.5GHz.

### 6.4 Summary

On-chip magnetic thin film inductors under external bias field were studied to evaluate inductor performance as well as the magnetic film properties including effective permeability and saturation field. The work provides an efficient in-situ method to test fabricated magnetic thin film around the inductor structure providing more accurate results compared to traditional large film measurements. As the films are patterned, saturation field changes accordingly due to magnetization loss and shape anisotropy field. Experiments show that films with finger structure have larger saturation field making them suitable for high current applications such as DC-DC converter.

# Chapter 7

# IN-PACKAGE RF AND POWER INDUCTORS ON ORGANIC SUBSTRATES FOR SYSTEM IN PACKAGE (SIP) APPLICATIONS

With the fast development of portable electronics, such as smart phone, ultrabook, as well as high performance computation, integrating discrete passive components, i.e. inductors and capacitors, in package to miniaturize the overall form factor has been demanded by System in Package (SiP) technology. Although extensive efforts have been made to incorporate magnetic materials to on-chip inductors, less attentions were given to the magnetic materials on package substrates mainly because magnetic properties could be affected by packaging substrate surface, stress and temperature resulting in unfavorable degradation of device performance. This chapter characterized soft amorphous Co-Zr-Ta-B films on standard organic package substrates including ABF and polyimide. Effects of substrate roughness and stress were analyzed and simulated which provide strategies for integrating Co-Zr-Ta-B into package inductors and improving inductors performance.

## 7.1 Characterizations of Magnetic Thin Films on Packaging Substrates

Amorphous Co-4%Zr-4%Ta-8%B (at. %) films were deposited with a constant DC magnetic field by DC magnetron sputtering on two kinds of organic packaging substrates, i.e. ABF and polyimide. The substrates investigated here are 500 µm thick commercial available polished polyimide substrate, 100 µm thick ABF laminated on glass substrate, along with our standard polished quartz substrate. Boron in Co-Zr-Ta-B film was also used to increase the film resistivity for high power density applications as in previous experiments. The unlaminated films were 500 nm thick while the laminated

films were ten 50 nm thick layers with a few nanometers of cobalt oxide insulation layers in between to reduce eddy current loss. Surface roughness effect was first examined by measuring the roughness of bare substrates and as-deposited Co-Zr-Ta-B films using optical profiler with high resolution, as shown in Table VIII.

TABLE VIII
ROUGHNESS OF CO-ZR-TA-B FILMS ON DIFFERENT SUBSTRATES (NM)

| | Bare | 500 nm Co-Zr-Ta-B | 50 nm × 10 Co-Zr-Ta-B |
|---|---|---|---|
| $SiO_2$/Si | -- | 9.3 | 7.7 |
| | -- | 9.5 | 8.2 |
| ABF/Glass | 33.9 | 28.4 | 21.4 |
| | 50.0 | 30.8 | 19.4 |
| Polyimide | 33.8 | 36.0 | 60.9 |
| | 35.0 | 38.5 | 63.2 |

Both ABF and polyimide substrates present tens of nanometer roughness, resulting in slightly sheared and broaden hysteresis loops compared to the films deposited on Si substrate. Measured hysteresis loops of Co-Zr-Ta-B are shown in Fig. 28. The coercivity of the two films on ABF/glass are all smaller than 1 Oe, see Table IX. The values are slightly larger but very similar to those on $SiO_2$/Si substrate, indicating their high quality. Similarly, the anisotropy $H_k$ are also similar to those on SiO2/Si. Overall, the quality and the softness of the Co-Zr-Ta-B films on ABF/glass remain the same as those deposited on SiO2/Si. However, the coercivity measured from polyimide substrate is larger than that from ABF substrate, especially for 500 nm film on polyimide, which is mainly due to the poor chamber vacuum during sputtering as a result of outgassing from polyimide substrate. Prebaking of polyimide substrates might be a possible solution for this out gassing issue.

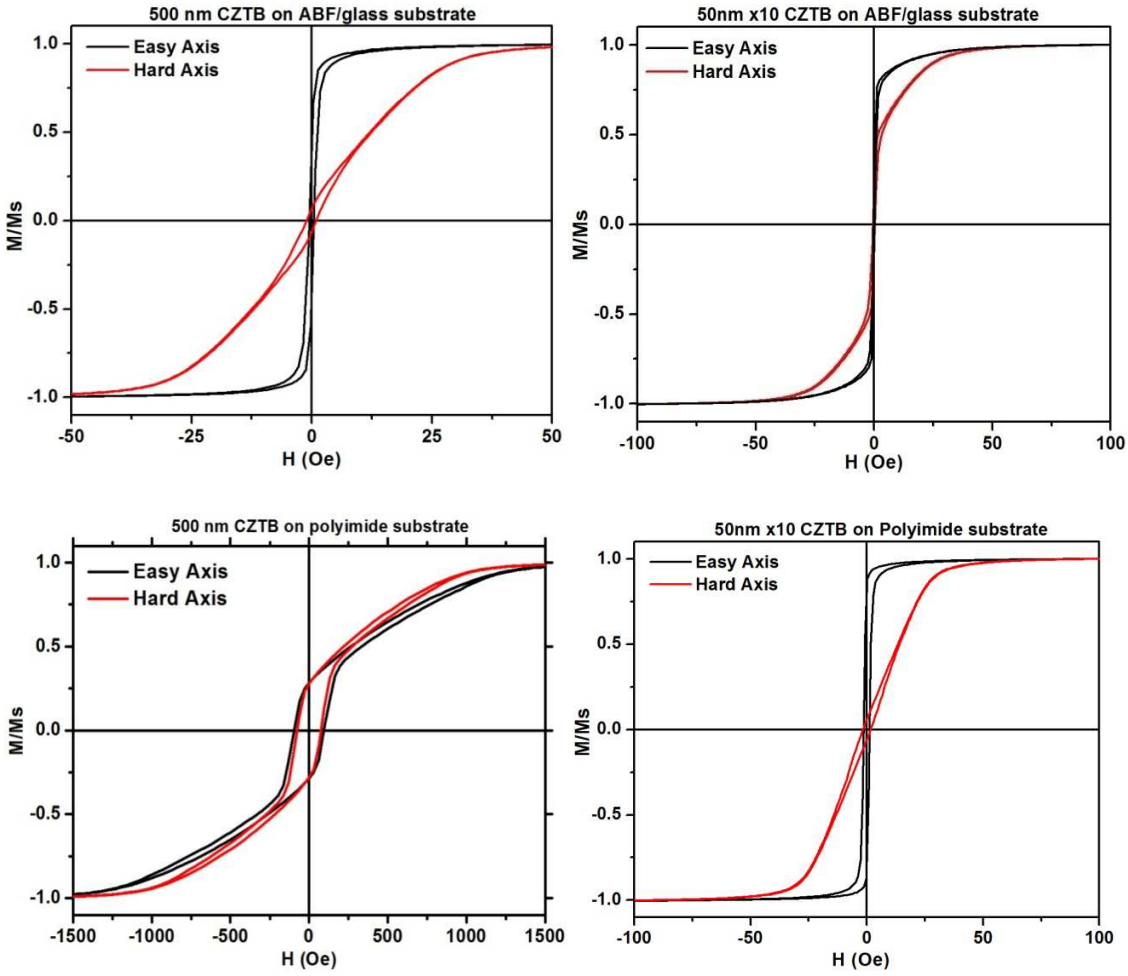


Fig. 28 Measured hysteresis loops of Co-Zr-Ta-B films on packaging substrates

The films were then annealed at 200 $^{o}$C in $N_2$ ambient for 2 hours with a DC magnetic field around 1000 Oe. No obvious improvement can be seen from the hysteresis loops, as shown in Fig. 29. For laminated films on both substrates, in-plane anisotropy tends to disappear after annealing which is partially due to the change of Co oxide insulation layers. Coercivity and anisotropy field are extracted from the hysteresis loops and listed in Table IX.

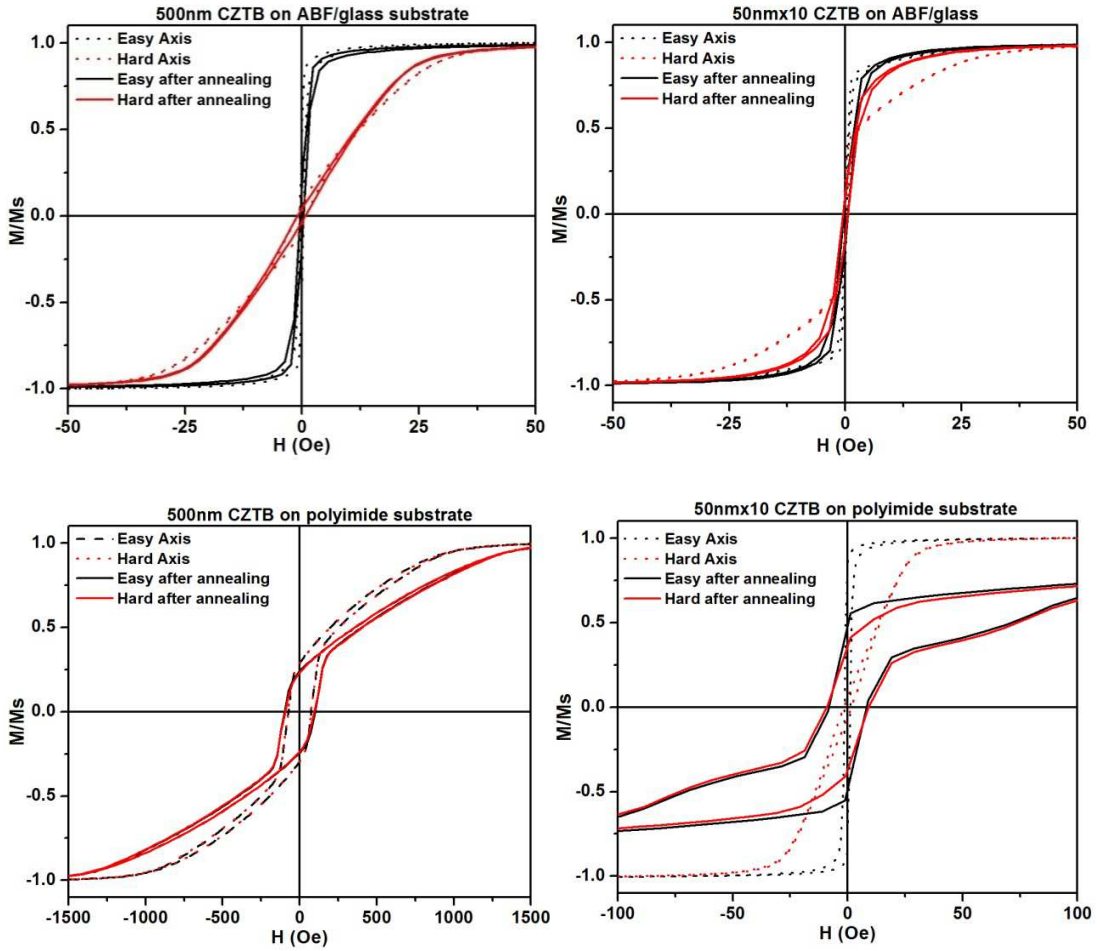


Fig. 29 Measured hysteresis loops of annealed Co-Zr-Ta-B films on packaging substrates

TABLE IX
$H_C$ AND $H_K$ OF CO-ZR-TA-B FILMS ON DIFFERENT SUBSTRATES (OE)

| | | 500 nm Co-Zr-Ta-B | | 50 nm × 10 Co-Zr-Ta-B | |
|---|---|---|---|---|---|
| | | as-deposit | annealed | as-deposit | annealed |
| $H_c$ in Easy Axis | $SiO_2$/Si | 0.1 | 0.1 | 0.18 | 0.05 |
| | ABF/glass | 0.4 | 0.4 | 0.25 | 0.5 |
| | Polyimide | 75 | 100 | 2.5 | 7 |
| $H_k$ in Hard Axis | $SiO_2$/Si | 17.8 | 19 | 22.5 | 21 |
| | ABF/glass | 27 | 24 | 27 | 15 |
| | Polyimide | -- | -- | 27 | -- |

## 7.2 Stress Analysis in Magnetic Films on Package Substrates

Stress in magnetic films has significant consequences for both device fabrication and performance. For device fabrication, large stress can cause deformation of inductor coils and package substrates such as warping, therefore is undesired. From a device performance perspective, stress in the magnetic films can introduce extra anisotropy resulting in magnetic properties deterioration. Before fabricating inductors with magnetic films on package substrates, it is necessary to analyze the stress in the magnetic films.

Film stress in magnetic films on or in package substrate was simulated by Abaqus FEA. Two types of structures were modeled with magnetic thin films on or in package substrates as seen in Fig. 30. It shows that for both structures large stress only occurs at the corners of the films. This indicates that there is no significant stress induced anisotropy in films which is helpful in keeping the uniaxial anisotropy of the magnetic film with high saturation field.

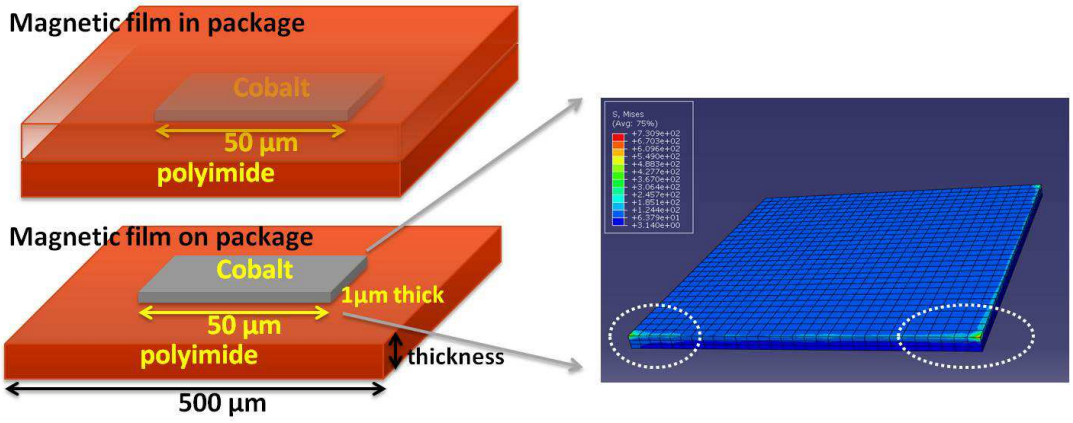


(a) (b)

Fig. 30 (a)Simulated structure with magnetic films in (top) and on (bottom) packaging substrates. (b)Stress mapping in magnetic films on packaging substrate.

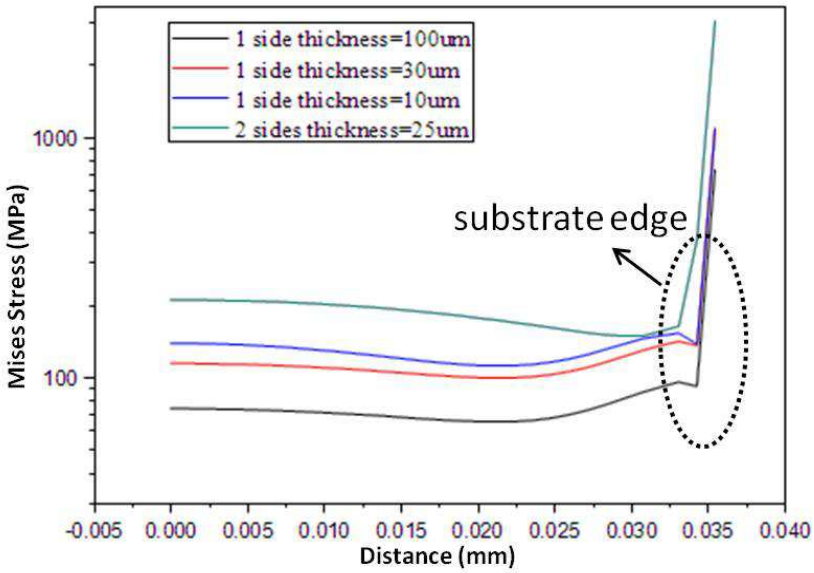


Fig. 31 Simulation of stress in magnetic films in and on packaging substrates showing large stress only occurs at substrate edges.

### 7.3 Inductors with Magnetic Films on Package Substrates

For demonstration of in-package magnetic thin film inductors the stripline inductors incorporating 500 nm thick Co-Zr-Ta-B film were fabricated using the identical procedure and conditions such as process temperatures onto three different substrates, quartz, polyimide and laminated ABF film on glass, using electron beam lithography (EBL) and magnetron sputtering for pattern definition and metallization, respectively, a standard procedure used in prior experiments. The typical fabricated stripline inductors without magnetic film, with film and with patterned magnetic film on ABF/glass substrate are shown in Fig. 32 (a), along with the schematic of the cross-section of the fabricated inductor and a representative scanning electron microscopy image. The length of the stripline inductor is 450 µm.

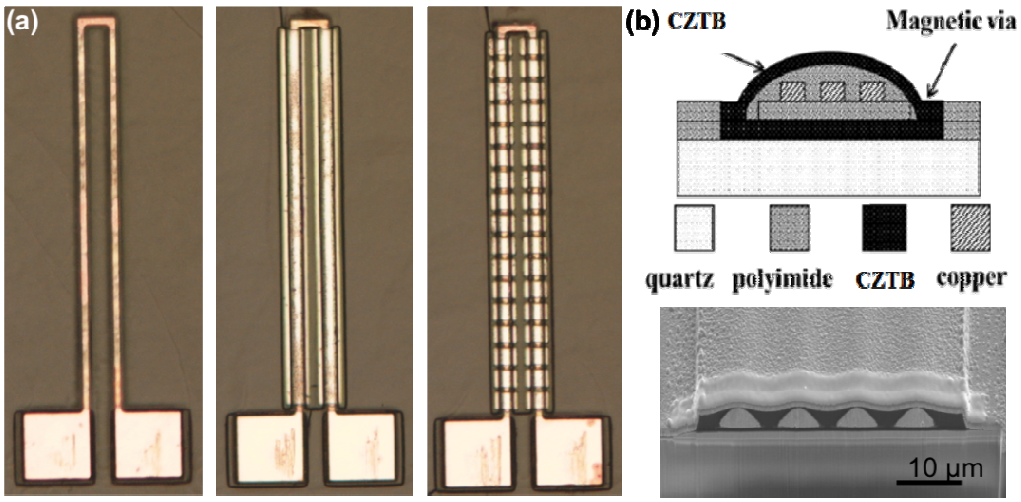


Fig. 32 Stripline inductor structure. (a) Pictures of fabricated bare, film and patterned Co-Zr-Ta-B film inductors on ABF films laminated on glass substrate. Length of the stripline inductor is 450 μm. (b) Schematic view of the cross-section of the inductor structure (top) and representative scanning electron microscopy image of the inductor cross-section (bottom).

Measurement of inductance and quality factor versus frequency of stripline inductors on three different substrates using non-laminated single layer 500 nm films are compared and shown in Fig. 33. With 500 nm thick non-laminated film the inductance increases to 2.7x, 1.6x, and 1.9x respectively, on quartz, polyimide and ABF/glass substrates compared to bare (air-core) inductors. All fabricated inductors show very good frequency response, with inductors on quartz substrate only showing near-constant value until sharp drop-off at frequency greater than 1 GHz, while inductance starting to decrease at around 1 GHz and 500 MHz respectively, for inductors on polyimide and ABF/glass. In the meantime, the quality factor of the inductor on polyimide and ABF/glass typically greater than, matches with those on quartz substrate. The slight smaller values in the inductance increase on polyimide and ABF/glass could due to rougher surface and the stress due to different materials involved in the inductor structure.

It is possible that repeated temperature cycles during the device fabrication process may have caused the stress in the magnetic film thus degrading the permeability and inductance increase. This effect, however, can be reduced if we introduce an intermediate layer between magnetic materials and packaging substrates. In addition, different substrate materials may lead to different thickness of spin-coated polyimide layer, which is used in the inductor as insulating layer. Such variations could affect magnetic layer structure, therefore the inductance values.

Field annealing was also performed on fabricated inductors on various substrate under these conditions: 200 °C for 2 hours under magnetic field estimated to be between 0.1 to 0.2 T. For inductor fabricated on ABF, this annealing did not degrade the performance of the inductors, with the same inductance value and quality factor. This indicates the robustness of the device, and it is promising to integrate inductor on packaging substrate, even with magnetic core materials integrated.

Spiral inductors with 500 nm Co-Zr-Ta-B films were fabricated on polyimide substrates with the same structure as the one on quartz substrate presented in Chapter 4. The air-core inductor maintains the theoretical inductance value of 1.9 nH indicating that the process on quartz substrates is fully compatible with organic packaging substrates. But for the inductors with magnetic materials, about 10% to 20% inductance enhancement was observed as shown in Fig. 34. Such low inductance increase is mainly due to the deterioration of the magnetic films which can be improved by the following ways. 1. Inserting an intermediate layer, such as spin-coated polyimide, between substrate and magnetic layer to reduce the possible thermal stress effect. 2. Reducing the process temperature, which is primarily determined by the curing temperature of

polyimide layers, in order to reduce the stress in the magnetic layer. 3. Extending the experience gained from fabricating inductors using CoZrTaB as magnetic layers to the incorporation of NiFe layers, as it is a commonly used material in many forms of inductors, including spiral, solenoid, and toroid structures, and one could therefore further evaluate the performance of such magnetic inductor on packaging substrate.

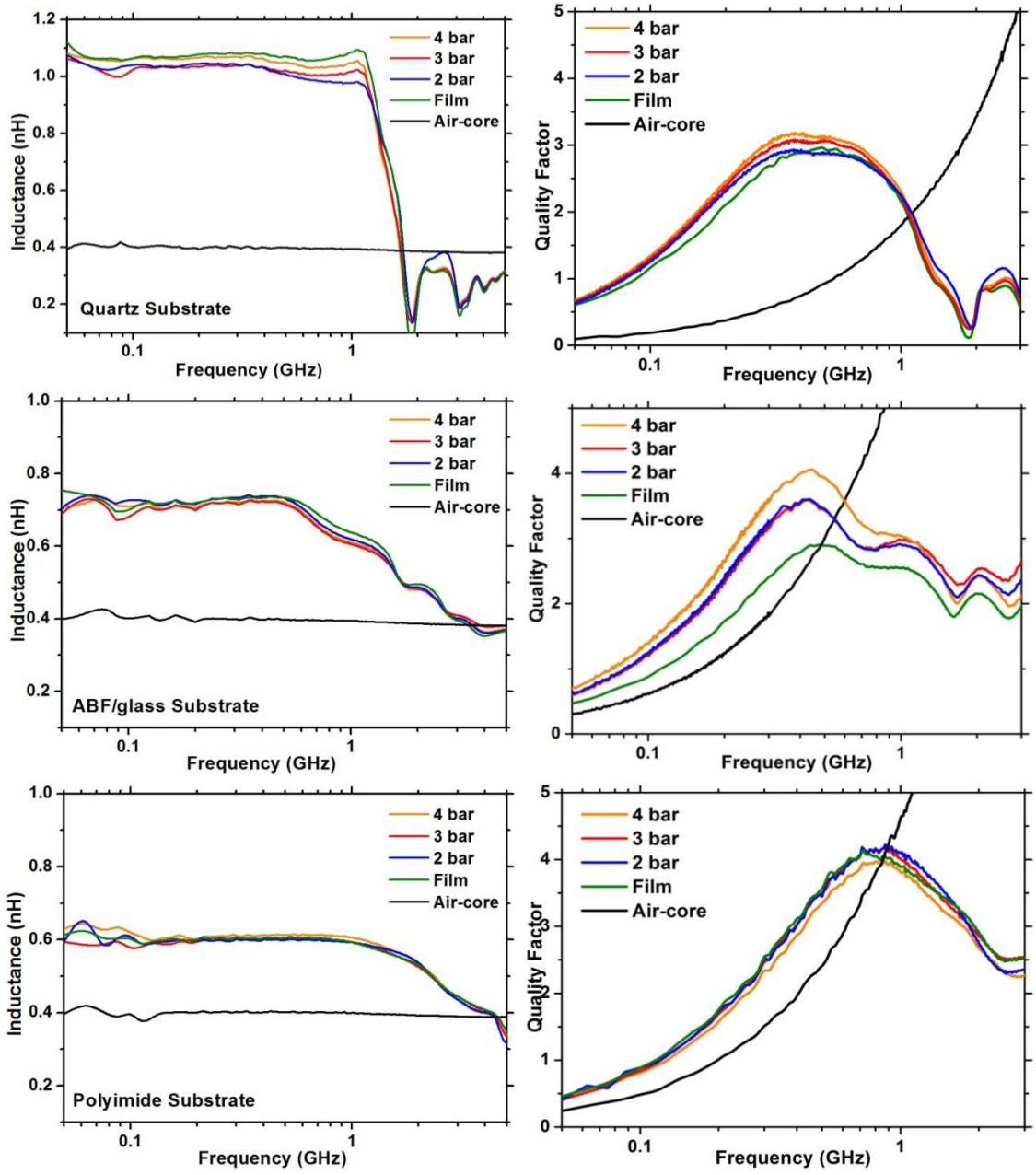

Fig. 33 Measured inductance and quality factor from stripeline inductors on different substrates.

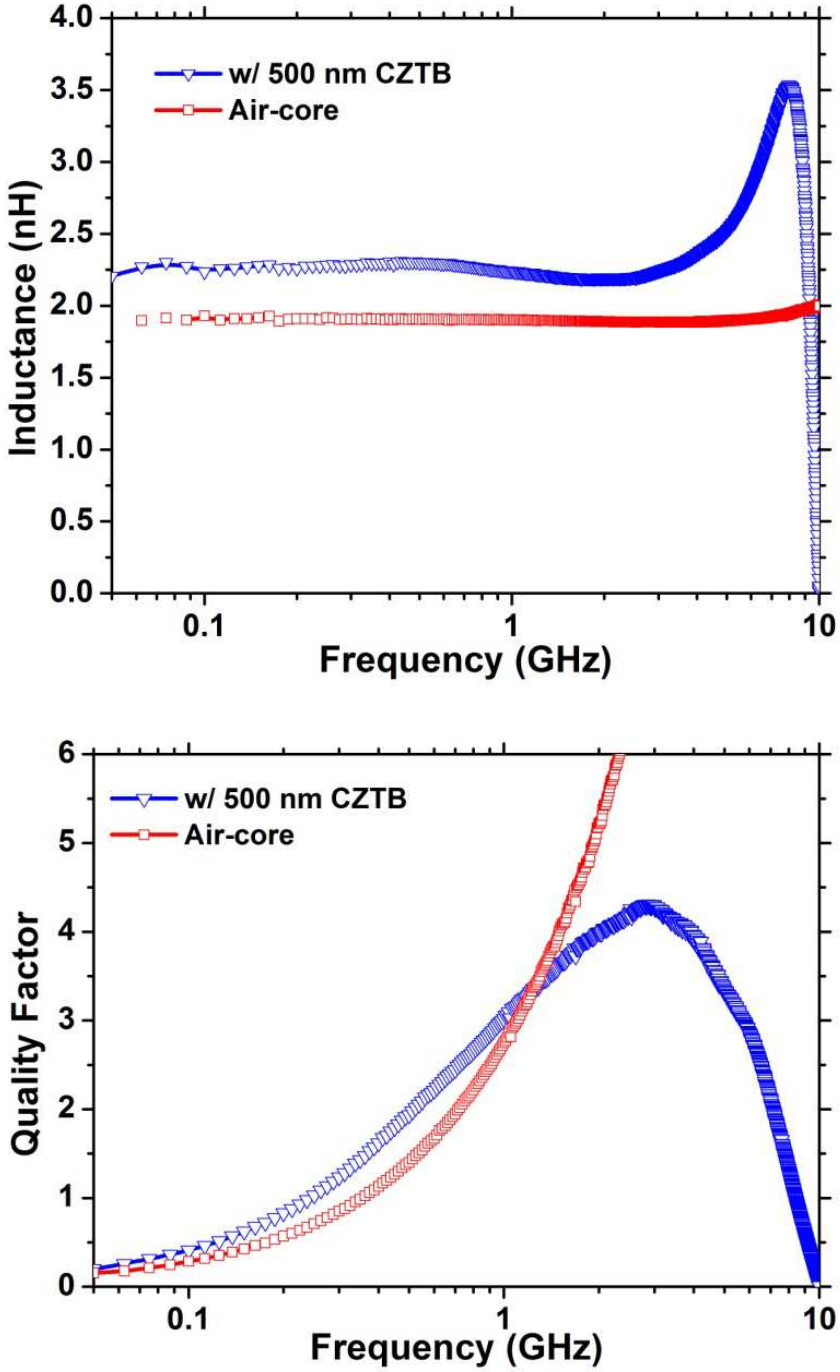


Fig. 34 Measured inductance and quality factor from spiral inductors on polyimide substrates.

# Chapter 8

## CONCLUSION

A systematic study of integrated inductor with micro-patterned magnetic materials used in System-in-Package (SiP) and System-on-Chip (SoP) technology was presented through 3D EM simulation to experiments. Effect of using high permeability magnetic materials with planar inductors to enhance the inductance density and quality factor was analyzed by extensive experimental and simulation study. It is demonstrated that by using laminated amorphous Co-Zr-Ta-B films, up to a 9.1X inductance increase with good frequency response up to 2 GHz can be achieved showing promising applications in RF circuits. Patterning effect of magnetic thin films was also investigated and then utilized in integrated inductors for optimized inductor performance. The role of magnetic vias in controlling magnetic flux and eddy current was analyzed based on which finger shaped magnetic vias were designed. Experiments demonstrate inductors with finger shaped magnetic vias not only have a peak quality factor above 1 GHz but also present a high saturation field around 325 Oe. Co-Zr-Ta-B films on standard organic package substrates were also characterized including ABF and polyimide substrates. Effects of substrate roughness and stress were analyzed and simulated which provide strategies for integrating Co-Zr-Ta-B into package inductors and improving inductors performance.

REFERENCES


[1] C. C. Tang, C. H. Wu, and S. I. Liu, "Miniature 3-D inductors in standard CMOS process," *Ieee Journal of Solid-State Circuits,* vol. 37, pp. 471-480, Apr 2002.

[2] S. A. Chickamenahalli, H. Braunisch, S. Srinivasan, H. Jiangqi, U. Shrivastava, and B. Sankman, "RF packaging and passives: design, fabrication, measurement, and validation of package embedded inductors," *Advanced Packaging, IEEE Transactions on,* vol. 28, pp. 665-673, 2005.

[3] J. N. Burghartz and B. Rejaei, "On the design of RF spiral inductors on silicon," *Ieee Transactions on Electron Devices,* vol. 50, pp. 718-729, Mar 2003.

[4] H. M. Hsu and M. M. Hsieh, "On-chip inductor above dummy metal patterns," *Solid-State Electronics,* vol. 52, pp. 998-1001, Jul 2008.

[5] C. L. Chua, D. K. Fork, K. Van Schuylenbergh, and L. Jeng-Ping, "Out-of-plane high-Q inductors on low-resistance silicon," *Microelectromechanical Systems, Journal of,* vol. 12, pp. 989-995, 2003.

[6] R. Foley, F. Waldron, J. Slowey, A. Alderman, B. Narveson, and S. C. O'Mathuna, "Technology roadmapping for Power Supply in Package (PSiP) and Power Supply on Chip (PwrSoC)," *Applied Power Electronics Conference and Exposition (APEC), 2010 Twenty-Fifth Annual IEEE,* pp. 525-532, 2010.

[7] C. H. Diaz, D. D. Tang, and J. Y. C. Sun, "CMOS technology for MS/RF SoC," *Electron Devices, IEEE Transactions on,* vol. 50, pp. 557-566, 2003.

[8] C. P. Yue and S. S. Wong, "On-chip spiral inductors with patterned ground shields for Si-based RF IC's," *Ieee Journal of Solid-State Circuits,* vol. 33, pp. 743-752, May 1998.

[9] M. Wens and M. Steyaert, *Design and implementation of fully-integrated inductive DC-DC converters in standard CMOS.* Dordrecht ; New York: Springer, 2011.

[10] A. Zolfaghari, A. Chan, and B. Razavi, "Stacked inductors and transformers in CMOS technology," *Solid-State Circuits, IEEE Journal of,* vol. 36, pp. 620-628, 2001.

[11] N. Zao, Z. Jing, F. Qiang, W. Xin, S. Zitao, Y. Yi, *et al.*, "Design and Analysis of Vertical Nanoparticles-Magnetic-Cored Inductors for RF ICs," *Electron Devices, IEEE Transactions on,* vol. 60, pp. 1427-1435, 2013.

[12] T. Hau-Yiu and J. Lau, "An on-chip vertical solenoid inductor design for multigigahertz CMOS RFIC," *Microwave Theory and Techniques, IEEE Transactions on,* vol. 53, pp. 1883-1890, 2005.

[13] Y. Xuehong, K. Minsoo, F. Herrault, J. Chang-Hyeon, K. Jungkwung, and M. G. Allen, "Silicon-Embedding Approaches to 3-D Toroidal Inductor Fabrication," *Microelectromechanical Systems, Journal of,* vol. 22, pp. 580-588, 2013.

[14] V. Korenivski, "GHz magnetic film inductors," *Journal of Magnetism and Magnetic Materials,* vol. 215, pp. 800-806, Jun 2000.

[15] C. R. Sullivan, "Integrating magnetics for on-chip power: Challenges and opportunities," in *Custom Integrated Circuits Conference, 2009. CICC '09. IEEE,* 2009, pp. 291-298.

[16] A. M. Crawford, D. Gardner, and S. X. Wang, "High-frequency microinductors with amorphous magnetic ground planes," *Ieee Transactions on Magnetics,* vol. 38, pp. 3168-3170, Sep 2002.

[17] B. Viala, A. S. Royet, R. Cuchet, M. Aid, P. Gaud, O. Valls, *et al.*, "RF planar ferromagnetic inductors on silicon," *Ieee Transactions on Magnetics,* vol. 40, pp. 1999-2001, Jul 2004.

[18] B. Viala, S. Couderc, A. S. Royet, P. Ancey, and G. Bouche, "Bidirectional ferromagnetic spiral inductors using single deposition," *Ieee Transactions on Magnetics,* vol. 41, pp. 3544-3549, Oct 2005.

[19] K. Kawabe, H. Koyama, and K. Shirae, "PLANAR INDUCTOR," *Ieee Transactions on Magnetics,* vol. 20, pp. 1804-1806, 1984.

[20] O. Oshiro, K. Kawabe, H. Tsujimoto, and K. Shirae, "A Wide Frequency Planar Inductor," *Magnetics in Japan, IEEE Translation Journal on,* vol. 2, pp. 331-332, 1987.

[21] O. Oshiro, H. Tsujimoto, and K. Shirae, "A Closed-Type Planar Inductor," *Magnetics in Japan, IEEE Translation Journal on,* vol. 2, pp. 329-330, 1987.

[22] M. Yamaguchi, S. Arakawa, H. Ohzeki, Y. Hayashi, and K. I. Arai, "CHARACTERISTICS AND ANALYSIS OF A THIN-FILM INDUCTOR WITH CLOSED MAGNETIC-CIRCUIT STRUCTURE," *Ieee Transactions on Magnetics,* vol. 28, pp. 3015-3017, Sep 1992.

[23] V. Korenivski and R. B. vanDover, "Magnetic film inductors for radio frequency applications," *Journal of Applied Physics,* vol. 82, pp. 5247-5254, Nov 1997.

[24] M. Yamaguchi, K. Suezawa, K. I. Arai, Y. Takahashi, S. Kikuchi, Y. Shimada, *et al.*, "Microfabrication and characteristics of magnetic thin-film inductors in the ultrahigh frequency region," *Journal of Applied Physics*, vol. 85, pp. 7919-7922, Jun 1 1999.

[25] M. Yamaguchi, M. Baba, and K. I. Arai, "Sandwich-type ferromagnetic RF integrated inductor," *Ieee Transactions on Microwave Theory and Techniques*, vol. 49, pp. 2331-2335, Dec 2001.

[26] D. S. Gardner, G. Schrom, P. Hazucha, F. Paillet, T. Karnik, S. Borkar, *et al.*, "Integrated on-chip inductors using magnetic material (invited)," *Journal of Applied Physics*, vol. 103, Apr 1 2008.

[27] C. Yang, F. Liu, X. Wang, J. Zhan, A. Wang, T. L. Ren, *et al.*, "Investigation of On-Chip Soft-Ferrite-Integrated Inductors for RF ICs-Part II: Experiments," *Ieee Transactions on Electron Devices*, vol. 56, pp. 3141-3148, Dec 2009.

[28] M. Yamaguchi, K. H. Kim, and S. Ikedaa, "Soft magnetic materials application in the RF range," *Journal of Magnetism and Magnetic Materials*, vol. 304, pp. 208-213, Sep 2006.

[29] S. Couderc, B. Viala, P. Ancey, G. Bouche, and R. Pantel, "FeHfN and FeHfNO soft magnetic films for RF applications," *Magnetics, IEEE Transactions on*, vol. 41, pp. 3319-3321, 2005.

[30] K. Ikeda, K. Kobayashi, K. Ohta, R. Kondo, T. Suzuki, and M. Fujimoto, "Thin-film inductor for gigahertz band with CoFeSiO-SiO<sub>2</sub> multilayer granular films and its application for power amplifier module," *Magnetics, IEEE Transactions on*, vol. 39, pp. 3057-3061, 2003.

[31] K. Seemann, H. Leiste, and C. Ziebert, "Soft magnetic FeCoTaN film cores for new high-frequency CMOS compatible micro-inductors," *Journal of Magnetism and Magnetic Materials*, vol. 316, pp. e879-e882, 9// 2007.

[32] C.-H. Lee, D.-h. Shin, D.-h. Ahn, S.-e. Nam, and H.-j. Kim, "Fabrication of thin film inductors using FeTaN soft magnetic films," *Journal of Applied Physics*, vol. 85, pp. 4898-4900, 1999.

[33] K. Seemann, H. Leiste, and V. Bekker, "New theoretical approach to the RF-dynamics of soft magnetic FeTaN films for CMOS components," *Journal of Magnetism and Magnetic Materials*, vol. 278, pp. 200-207, 7// 2004.

[34] K. Shirakawa, H. Kurata, J. Toriu, H. Matsuki, and K. Murakami, "A new planar inductor with magnetic closed circuit," *Magnetics, IEEE Transactions on*, vol. 27, pp. 5432-5434, 1991.

[35] K. Shirakawa, K. Yamaguchi, M. Hirata, T. Yamaoka, F. Takeda, K. Murakami, *et al.*, "Thin film cloth-structured inductor for magnetic integrated circuit," *Magnetics, IEEE Transactions on,* vol. 26, pp. 2262-2264, 1990.

[36] Y. Zhuang, M. Vroubel, B. Rejaei, and J. N. Burghartz, "Integrated RF inductors with micro-patterned NiFe core," *Solid-State Electronics,* vol. 51, pp. 405-413, Mar 2007.

[37] L. Liangliang, L. Dok Won, H. Kyu-Pyung, M. Yongki, T. Hizume, M. Tanaka, *et al.*, "Small-Resistance and High-Quality-Factor Magnetic Integrated Inductors on PCB," *Advanced Packaging, IEEE Transactions on,* vol. 32, pp. 780-787, 2009.

[38] J. Mullenix, A. El-Ghazaly, and S. X. Wang, "Integrated Transformers With Sputtered Laminated Magnetic Core," *Magnetics, IEEE Transactions on,* vol. 49, pp. 4021-4027, 2013.

[39] Q. Jizheng, D. V. Harburg, and C. R. Sullivan, "A toroidal power inductor using radial-anisotropy thin-film magnetic material based on a hybrid fabrication process," in *Applied Power Electronics Conference and Exposition (APEC), 2013 Twenty-Eighth Annual IEEE*, 2013, pp. 1660-1667.

[40] C. Kittel, "ON THE THEORY OF FERROMAGNETIC RESONANCE ABSORPTION," *Physical Review,* vol. 73, pp. 155-161, 1948.

[41] W. Xu, "On-chip inductor with integrated magnetic material," Ph D, Arizona State University, 2010.

[42] T. Dastagir, W. Xu, S. Sinha, H. Wu, Y. Cao, and H. B. Yu, "Tuning the permeability of permalloy films for on-chip inductor applications," *Applied Physics Letters,* vol. 97, Oct 2010.

[43] D. S. Gardner, G. Schrom, P. Hazucha, F. Paillet, T. Karnik, and S. Borkar, "Integrated on-chip inductors with magnetic films," *Ieee Transactions on Magnetics,* vol. 43, pp. 2615-2617, Jun 2007.

[44] P. R. Morrow, C. M. Park, H. W. Koertzen, and J. T. DiBene, "Design and Fabrication of On-Chip Coupled Inductors Integrated With Magnetic Material for Voltage Regulators," *Ieee Transactions on Magnetics,* vol. 47, pp. 1678-1686, Jun 2011.

[45] P. Herget, N. G. Wang, E. J. O'Sullivan, B. C. Webb, L. T. Romankiw, R. Fontana, *et al.*, "A Study of Current Density Limits Due to Saturation in Thin

Film Magnetic Inductors for On-Chip Power Conversion," *Ieee Transactions on Magnetics,* vol. 48, pp. 4119-4122, Nov 2012.

[46] A. Aharoni, "Demagnetizing factors for rectangular ferromagnetic prisms," *Journal of Applied Physics,* vol. 83, pp. 3432-3434, 1998.

[47] A. Aharoni, L. Pust, and M. Kief, "Comparing theoretical demagnetizing factors with the observed saturation process in rectangular shields," *Journal of Applied Physics,* vol. 87, pp. 6564-6566, May 2000.

[48] Y. Li, Y. R. Lu, and W. E. Bailey, "Single-domain shape anisotropy in near-macroscopic Ni80Fe20 thin-film rectangles," *Journal of Applied Physics,* vol. 113, May 2013.

[49] R. Engel-Herbert and T. Hesjedal, "Calculation of the magnetic stray field of a uniaxial magnetic domain," *Journal of Applied Physics,* vol. 97, Apr 2005.

[50] W. Xu, H. Wu, D. S. Gardner, S. Sinha, T. Dastagir, B. Bakkaloglu, *et al.*, "Sub-100 mu m scale on-chip inductors with CoZrTa for GHz applications," *Journal of Applied Physics,* vol. 109, p. 3, Apr 2011.

[51] E. vandeRiet and F. Roozeboom, "Ferromagnetic resonance and eddy currents in high-permeable thin films," *Journal of Applied Physics,* vol. 81, pp. 350-354, Jan 1997.

[52] D. S. Gardner, G. Schrom, F. Paillet, B. Jamieson, T. Karnik, and S. Borkar, "Review of On-Chip Inductor Structures With Magnetic Films," *Ieee Transactions on Magnetics,* vol. 45, pp. 4760-4766, Oct 2009.

[53] M. Yamaguchi, K. Suezawa, Y. Takahashi, K. I. Arai, S. Kikuchi, Y. Shimada, *et al.*, "Magnetic thin-film inductors for RF-integrated circuits," *Journal of Magnetism and Magnetic Materials,* vol. 215, pp. 807-810, Jun 2000.

## BIOGRAPHICAL SKETCH

Hao Wu was born in HuaiAn, Jiangsu, China, in 1983. He received the B.S. degree in Electrical Engineering from Nanjing University, Nanjing, China in 2006 and the M.S. degree in Microelectronics from Tsinghua University, Beijing, China in 2009. From 2009 to 2013 he studied for a Ph.D. degree in Electrical Engineering with Ira A. Fulton Schools of Engineering, Arizona State University, Tempe, AZ.

Hao's research work is mainly on the design, simulation, optimization, fabrication and testing of on-chip magnetic thin film inductors with integrated soft magnetic materials including Ni-Fe, Co-Zr-Ta and Co-Zr-Ta-B. He has employed new strategies to engineer ferromagnetic resonance (FMR) properties of the materials, and to understand the effects of magnetic materials shape, size on the inductor performance. His research interests are also including thin film growth/characterization and nanowire based MOSFET devices.

During his Ph.D. study, Hao has published eight journal papers, more than ten conference presentations and co-authored one book chapter. His achievement was recognized by the IEEE Magnetic Society, as he was selected as a finalist in the competition for the Best Student Award at IEEE International Magnetics Conference (INTERMAG) in May 2012 in Vancouver, Canada.